A NETWORK MODEL OF THE NEOCORTEX ACCOUNTING FOR ITS LAMINAR STRUCTURE

BACHLOR THESIS

submitted by

FRIEDRICH SCHUESSLER

July 30, 2015

Prof. Dr. Jens Timmer

Fakultät für Mathematik und Physik

ALBERT-LUDWIGS-UNIVERSITÄT

Freiburg im Breisgau

ERKLÄRUNG

Hiermit versichere ich, die eingereichte Bachelorarbeit selbstständig verfasst und keine anderen als die von mir angegebene Quellen und Hilfsmittel benutzt zu haben. Wörtlich oder inhaltlich verwendete Quellen wurden entsprechend den anerkannten Regeln wissenschaftlichen Arbeitens (lege artis) zitiert. Ich erkläre weiterhin, dass die vorliegende Arbeit noch nicht anderweitig als Bachelorarbeit eingereicht wurde.

Freiburg im Breisgau, 30. Juli 2015

Friedrich Schuessler

CONTENTS

LIST OF FIGURES

LIST OF TABLES

1 INTRODUCTION

ONE OF THE CENTRAL objectives of the current research in computational neuroscience is the understanding of the neocortex, the part of the mammalian brain most frequently associated with higher cognitive functions [4]. The approach of linking the function of the brain to its structure faces a large difficulty: Due to the vast number of details over a large number of scales, it is not clear what level of abstraction is adequate for a specific phenomenon. A promising choice is to focus on substructures of the neocortex, as some of the experimental findings of the past suggest: Important insights into the cortical architecture date back to the beginning of the 20th century, when the anatomist Brodmann [7] discovered two key features found in all mammals: a subdivision into cytoarchitecturally distinguishable regions as well as the subdivision into six horizontal layers. Many of Brodmann's areas are now known to coincide with functional areas as well, with the best studied example being area 17 corresponding to V1 of the visual cortex [4]. The layers are distinguished by both neuron types and neuronal connections, and are thought to have different roles in processing information. In V1, for example, the visual input enters via three different pathways which are further associated with the analysis of object motion, shape and color, respectively [4]. In 1957, almost fifty years after Brodmann's discoveries, Mountcastle [20] put forward another suggestion central for todays view on the neocortex: According to his hypothesis of columnar functional organization, neurons with horizontal distances of more than 500 µm do not share common sensory receptive fields. On one side, this theorized canonical microcircuit is still not found experimentally and the very idea of it being a functional unit strongly debated (see e. g. Horton and Adams [15] for a review). The groundbreaking work of Hubel and Wiesel [16] on information processing in the visual system during the 1960s and 1970s, on the other hand, contributed much to the establishment of the notion of columnar organization. Until today it remains a widely adopted hypothesis for explaining information processing within the cortex [10].

Even though computational neuroscience relies heavily on experimental data, the distinguishing aspect of the discipline is the usage of mathematical models for analysis and predictions. One set of these models is concerned with the behavior of large scale networks with spiking neurons as the basic constituents. A paradigmatic model neuron has been introduced by Hodgkin and Huxley [14] in 1952 on the basis of examining the squid giant axon. Their model describes the generation of action potentials on the basis of voltage-gated ion channels. Remarkably, however, it is a much simpler model which is been chosen over the biologically more realistic Hodgkin–Huxley model: Almost fifty years earlier and not yet aware of the physiological details of action potential generation, Lapicque [19] put forward the integrate-and-fire model. He modelled a spiking neuron by a simple circuit with parallel resistor and capacitor and a threshold at which a prototypical spike is emitted. The extension by including a leaky term mimics diffusion of ions through the membrane. this model has not much changed until today – indeed, it has even been shown to be the superior choice over biologically much more realistic models in many cases [6]. The model neurons are linked by synapses to form a spiking network model. Often, the choice of a synapse model is an equally simple basic model, implying either instant changes of the membrane potential at the arrival of the spike (voltage based or δ-synapses) or an injection of current following a specific curve in time (e. g. exponential or α-synapses). While the prior choice is easier to handle analytically, the latter is often preferred as the biologically more realistic choice. Despite the simplicity of its basic components, the networks can show a highly complex behaviour and may be strongly dependent on a specific choice of parameters. Specifically, modeling a network, one has to take into account the possibility of runaway activity in the case of too much excitation. A common choice suggested both by stability arguments as well as experimental evidence is to construct networks including inhibitory populations. In accordance with anatomical estimates, the excitatory populations are frequently much larger.[1] The stability is then reached by assigning larger weights to the inhibitory synapses until balance or dominating inhibition is reached. As the resulting mathematical models are often too complex to be described solely analytical, many studies rely heavily on numerical simulations. Apart

1 The estimates for the cortex are roughly 80 % excitatory and 20 % inhibitory neurons.[8]

from computational power both becoming less costly and more powerful, this set of tools is also becoming increasingly convenient due to development on the software side. One important example in this area is the NEST neural simulation tool, initially developed by Gewaltig and Diesmann [13]. Simulations are defined in the stack-based simulation language SLI, but since 2008 an interface for the Python programming language [27] is available.

In order to consolidate experimental data with the abstract models, the available anatomical studies have to be taken into account and in many cases made comparable in the first place. This has been done for a spiking network model of the neocortical microcircuit that supplied the basis for this thesis: A recent work of Potjans and Diesmann [24] includes both laminar and columnar organization and utilizes numerous studies estimating the number of synapses between different populations in order to construct an integrated connectivity map.[2] The network represents a column with a surface of 1.0 mm^2 containing eight populations of neurons organized in four layers[3], each with an excitatory and an inhibitory population, subsuming different neuron types under these two. The synapses connecting the neurons are drawn randomly with probabilities according to the connectivity map. A central result of this study was the reproduction of firing rates measured in a variety animal models.

Parallel to the development of increasingly sophisticated spiking network models, an analytical framework describing populations of integrate-and-fire neurons has been developed. While a number of results have been published thirty to forty years ago (e. g. Ricciardi [26] and Tuckwell [32]), a mayor landmark in this field has been introduced by Brunel [8] at the verge of the current century. Using a diffusion approximation and assuming uncorrelated input to each neuron, he developed a mean field theory for the firing rates and characterized different states a generic model of two populations can exhibit. Most prominently, he established the notion of a network state where neurons fire both irregularly in time and asynchronously. This state, coined *asynchronous irregular (AI) state*, is considered to be

2 The experimental studies utilized in the study both for connectivity and firing stem from various animal models, showing that the data available is still sparse and interpretation of the results has to be done with cautiously.

3 Two of the six layers are subsumed into one, the uppermost layer, is omitted. This latter one is also called the molecular layer because it does not contain a significant number of cells [4].

analogous to what is found in experiments observing the cortical activity in awake and active animals.[4] Although it is not in general clear to what level of complexity the theory can by extended, it has been utilized in a number of studies with different foci and shown to be a suitable tool.[5] Finally, the developed mean field theory not only has the possibility to predict firing rates, it may also be seen as a tool seeking a deeper understanding of how information is processed within neural networks. A very fundamental question is whether information is encoded in firing rates or in exact spike times and correlations. Answering this basic question may be considered a milestone towards more complex ones relating to such highly emergent phenomena as higher cognitive tasks or perception.

THIS STUDY SURROUNDS TWO central hypotheses. At first, an implementation of the microcircuit model by Potjans and Diesmann in the framework of PyNEST is expected to reproduce the same results as the available original implementation written in SLI. Due to internal differences in the application of random numbers, the demanded agreement will only be of statistical quality. The measures used for the validation are common quantities for the characterization of the network activity and will also enter in the next section of this study. The second part is built upon the proposition that the mean field theory can be extended and applied to the microcircuit model. A number of quantities are predicted by the theory and will be compared with the data obtained from simulations. As the spiking network model and the mean field theory do not employ the same constituents, some deviations are expected to stem from these differences.

THE THESIS IS STRUCTURED as follows. The first section contains a detailed account of the spiking network model as well as a derivation of the mean field model for eight neuron populations. The results are then presented comparing the simulation results to those of the implementation of the original publication by Potjans and Diesmann [24] as well as a closer look on the statistical properties of spike trains within one population. This is followed by comparing simulation results to

4 Cf. El Boustani et al. [12] for a discussion comparing experimental data and theoretical predictions.

5 See for example Sadeh and Rotter [29] for an application regarding orientation selectivity.

those obtained with the mean field model. An example varying the inhibitory synaptic strength shows that the mean field model is a convenient tool for predictions. The results are summarized and discussed in the final section.

2

METHODS

2.1 SPIKING NETWORK MODEL

A FUNDAMENTAL ASPECT that constitutes the basis of natural sciences is the reproducibility of results. Applying this paradigm to computational neuroscience, it turns out that a detailed description of the constituents, the connections and implementation of the network models is vital. Following Nordlie et al.'s. [23] suggestions on "good model description practice", the network model is described in in a top-down manner over the following paragraphs while a detailed overview is provided in two tables: Table 1 summarizes the structure whereas specific numerical values of the parameters are shown in Table 2.

THE NETWORK CONSISTS of eight cortical populations arranged in four layers. Each layer contains an excitatory as well as an inhibitory population, implying what is known as Dale's principle: neurons can only be of one type or the other.[1] A simplified diagram of the network together with an illustration of population sizes is given in Figure 1. A total of 77169 leaky integrate-and-fire neurons are distributed according to the population sizes given in Table 2. The total numbers of excitatory and inhibitory neurons are 61843 and 15326, respectively, yielding a ratio of 4.04 of excitatory over inhibitory neurons.

Synapses are created according to a set connection rule, referred to as "fixed total number": For each combination of pre- and postsynaptic population, pairs of neurons to be connected are drawn randomly until a fixed number of synapses is reached, allowing for multiple synapses and self-connections. Potjans and Diesmann's original model defines the connection probability $P_{\text{conn},ab}$ of one neuron in the presynaptic population a to form at least one connection with one neuron in the postsy-

1 The actual principle is aimed at more detailed models, hence more specific stating that "at all the axonal branches of a neuron, there was liberation of the same transmitter substance or substances" [11].

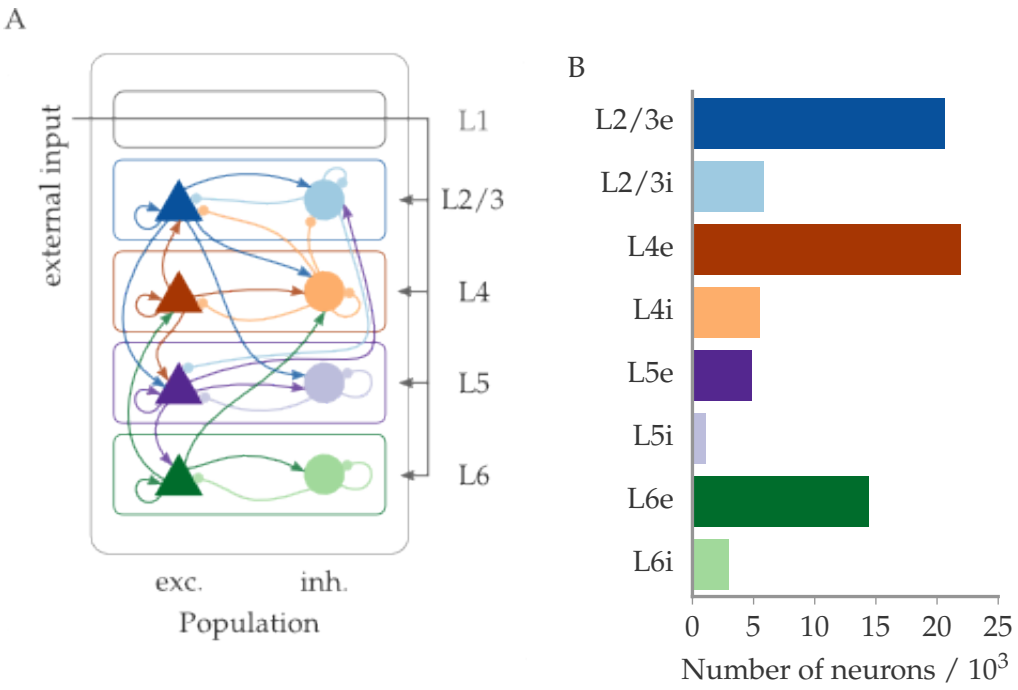

Figure 1: Description of the network model. (**A**) Diagram of the layered cortical network. Layers 2/3, 4, 5, and 6 are composed of one excitatory (triangles) and one inhibitory population (circles) each. The connections are only shown for probabilities > 0.04. The external input is simulated by Poissonian spike trains with adapted rates for each population. Layer 1 does not contain neuron populations. (**B**) Population sizes, total of 77169 neurons. The total number of inhibitory neurons is roughly 1/4 of the number of excitatory neurons.

naptic population b. For given population sizes N_a and N_b, the number of synapses C_{ab} is then calculated by

$$C_{ab} = \frac{\ln\left(1 - P_{\text{conn},ab}\right)}{\ln\left(1 - \frac{1}{N_a N_b}\right)}, \tag{1}$$

the inverse of the formula for connection probabilities of the original study [24].

The weight w for each synapse is drawn from a normal distribution. For excitatory presynaptic neurons, this mean value is set to $87,8$ pA (see below for a derivation). The mean for inhibitory ones is determined by multiplying with a factor $-g$, where the relative inhibitory synapse strength is set to $g = 4$. There is one important exception to this scheme: The mean for the connection from L4e to L2/3e is increased by a factor

of $j_{02} = 2$ (consult [24] for details). The standard deviation is set to 10% of the mean. The distributions from which weights are drawn are clipped, such that a neuron assigned to the excitatory population will not have associated outgoing synapses with $w < 0$ and vice versa for inhibitory ones. Delays are drawn from normal distributions as well, with a mean value of 1.5 ms for excitatory presynaptic neurons and half this value for inhibitory ones. The relative standard deviation is set to 50 %. The distributions are again clipped such that $d \geqslant 0$

The neurons are leaky integrate-and-fire neurons with a fixed voltage threshold. Below the threshold θ, the dynamics of the membrane potential $V_i(t)$ for neuron i are governed by the differential equation

$$\tau_m \frac{dV_i(t)}{dt} = -(V_i(t) - E_L) + \frac{\tau_m}{C_m} I_i(t)\,. \tag{2}$$

The membrane is specified by its resting potential E_L, its time constant τ_m and the capacitance C_m. If, at time t, the threshold is reached, the neuron emits a spike and remains in a refractory period for a fixed time τ_{rp}, with the membrane potential set to V_r and discarding any input arriving. The total input to the neuron is represented by the current $I_i(t)$, which is a linear superposition of the individual postsynaptic currents (PSC) of the recurrent network.

The model implements postsynaptic current synapses with exponential shape, such that each spike arriving at one neuron leads to a current

$$I_{syn}(t) = w \exp\left(\frac{-t}{\tau_{syn}}\right) \tag{3}$$

where w is the weight of the synapse in the model, which corresponds to the amplitude of the PSC at the time the spike arrives. τ_{syn} is the synaptic time constant. Since measuring currents remains a difficult task for experimentalists, the model relays on measurements of the amplitude of the postsynaptic potential (PSP). In order to use the experimental observations, an approximative transformation is implemented. The PSC induced by one spike of given PSP with the membrane potential at rest is calculated as follows: For $E_L = 0$, setting $I(t) = I_{syn}(t)$ in equation (2) yields:

$$\dot{V}(t) = -\frac{1}{\tau_m} V(t) + \frac{w}{C_m} \exp\left(-\frac{t}{\tau_{syn}}\right). \tag{4}$$

This has the solution

$$V(t) = -\frac{w\tau_m\tau_{syn}}{C_m\left(\tau_m - \tau_{syn}\right)} \exp\left(-\frac{t}{\tau_{syn}}\right) + C_1 \exp\left(-\frac{t}{\tau_m}\right) \quad (5)$$

with integration constant C_1. When applying the boundary condition $V(t = 0) = 0$, this constant is set to

$$C_1 = \frac{w\tau_m\tau_{syn}}{C_m\Delta\tau} \quad (6)$$

where $\Delta\tau := \tau_m - \tau_{syn}$ is introduced. Thus

$$V(t) = C_1\left[\exp\left(-\frac{t}{\tau_m}\right) - \exp\left(-\frac{t}{\tau_{syn}}\right)\right]. \quad (7)$$

In order to get the peak PSP, we search for the maximum. Setting $\dot{V}(t) = 0$ yields

$$t_{max} = \ln\left(\frac{\tau_{syn}}{\tau_m}\right)\left(\frac{1}{\tau_m} - \frac{1}{\tau_{syn}}\right)^{-1}. \quad (8)$$

Inserting into equation (7) leads to

$$V(t_{max}) = \frac{w\tau_m\tau_{syn}}{C_m\Delta\tau}\left[\left(\frac{\tau_{syn}}{\tau_m}\right)^{\frac{\tau_{syn}}{\Delta\tau}} - \left(\frac{\tau_{syn}}{\tau_m}\right)^{\frac{\tau_m}{\Delta\tau}}\right]. \quad (9)$$

For a given PSP amplitude, this equation is simply inverted in order to get the according weight w. The value used for the original model and also applied in this work is 0.15 mV. It is suggested by experiments and yields a synaptic weight of 87.8 pA. Finally, the input current of neuron i can be described as the sum over currents induced by arriving spike trains,

$$I_i(t) = \sum_j w_{ij} \sum_k \exp\left(\frac{t - t_j^k - d_{ij}}{\tau_{syn}}\right), \quad (10)$$

where t_j^k is the time the k-th spike by neuron j was emitted and the delay between neuron i and j is set to d_{ij}.

THE ACTIVITY OF THE NETWORK depends both on the recurrent stimulation as well as a external input. Due to the inhibitory population balancing excitation, the model can exhibit a stable state. However, the presence of inhibition requires that the network is supplied with external stimuli – without this, it converges to quiescence [8]. In the case of the local neocortical

microcircuit, the roles of different external input and recurrence is debated widely. While some interpret the local circuit as computational building blocks [24], others focus on the interplay between different cortical regions (e. g. Boucsein et al. [5]). The model implemented in this work is only driven by unspecific input mimicking stimulation from close and distant cortical areas [24].[2]

Instead of using simulated neurons populations, the input is implemented as Poissonian spike trains. The underlying Poisson process with mean rate ν is a stochastic process formally defined as a continuous-time counting process $N(t), t \leqslant 0$ with the properties [32]

- $N(0) = 0$;
- for any $0 = t_0 < t_1 < t_2 < \cdots < t_{n-1} < t_n$, the random variables $N(t_k) - N(t_{k-1}), k = 1, 2, \ldots, n$ are mutually independent;
- for any $0 \leqslant t_1 < t_2, N(t_1) - N(t_2)$ is a Poisson random variable with probability distribution

$$\Pr\{N(t_2) - N(t_1) = k\} = \frac{(\nu(t_2 - t_1))^k \exp(-\nu(t_2 - t_1))}{k!} \tag{11}$$

  for $k \in \mathbb{N}$.

For the random variable $N(t_2) - N(t_1)$, mean and variance are given by $E[N(t_2) - N(t_1)] = \mathrm{Var}(N(t_2) - N(t_1)) = \nu(t_2 - t_1)$, such that the average number of spikes $\langle k \rangle$ per time bin of width $\Delta t = t_2 - t_1$ is

$$\frac{\langle N \rangle}{\Delta t} = \nu\,. \tag{12}$$

Furthermore, as mean and variance for the Poisson process are equal, the often cited Fano factor

$$F = \frac{\sigma^2}{\mu}\,, \tag{13}$$

defined for a random process with mean μ and variance σ, is equal to one.

2 The original publication included thalamic input in order to examine temporal transmission of stimuli. This is omitted here as the focus lies on stationary states.

In the spiking network model, each neuron receives spikes of a defined weight with the spike times implemented as such a Poisson process. All processes are mutually independent and the rate of each one is determined by a global background rate of 8 Hz multiplied by an external indegree $(C_{ext})_a$ for population a. This mimics a multiple number of synapses to the respective neuron, each receiving an independent Poisson process with a mean rate of 8 Hz.

At creation, the neurons are initialized by drawing their membrane potential from a normal distribution with mean -58 mV and a standard deviation of 10 mV. The activity of the network is measured in terms of spike trains (measuring the spike times of single neurons up to the maximal grid resolution h) and membrane potentials in mV. The results in this thesis are based on recording only a fraction of the neurons in the network, choosing n_a random neurons of each population a. If not specified else, spikes are recorded from 1000 neurons of each population, membrane potentials from 100. The further analysis of the data is explained in following sections. The large number of free parameters of the model and their chosen values are summarized in Table 2.

IN ORDER TO VERIFY that the model behaves reasonably, we examine a number of basic parameters before stating more central results. As the implementation of the neuron model is part of the NEST software and thus well established, the validation starts at the level of connections. Figure 2 shows the number of synapses for each pair of pre- and postsynaptic population and the mean number of synapses each neuron receives from a specific population. The total number of synapses in the model is almost 0.3 billion synapses.

With the connection rule "fixed total number" applied in the simulation, the number of synapses per postsynaptic neuron is expected to follow a binomial distribution: For pre- and postsynaptic populations a and b, respectively, each time a pair is drawn, one postsynaptic neuron is chosen with a probability $1/N_b$, N_b being the population size. This is repeated until C_{ab} synapses are created. Choosing one neuron the first k times and not again has the probability $\Pr\{X = k\} = \left(\frac{1}{N_b}\right)^k \left(1 - \frac{1}{N_b}\right)^{C_{ab}-k}$. Multiplied by the number of possibilities to choose this neu-

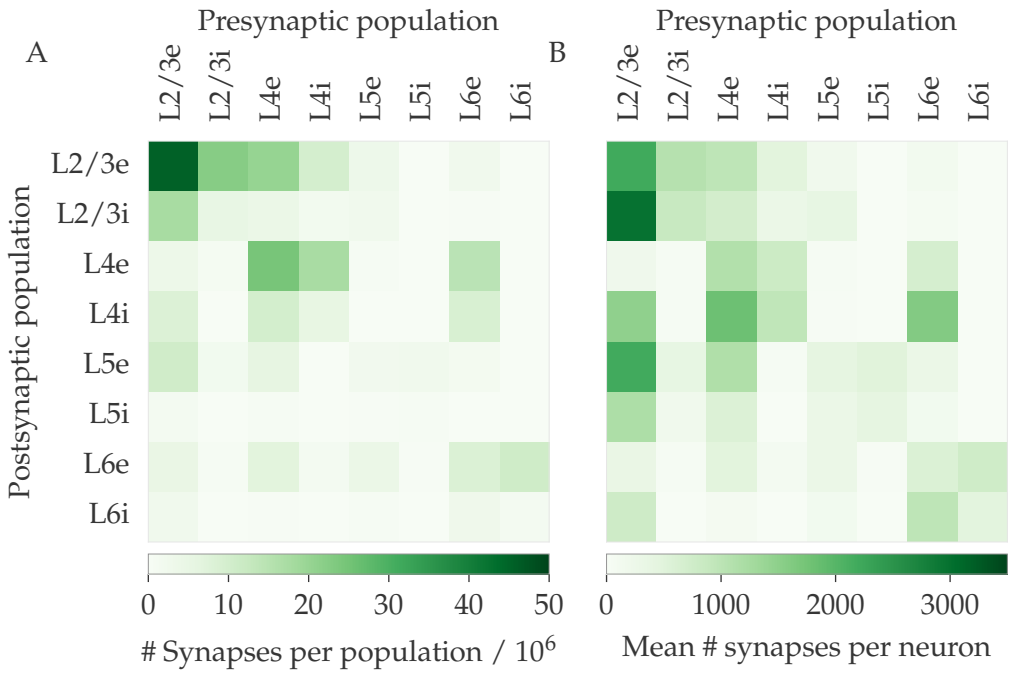

Figure 2: Connection between populations. (**A**) Calculated total synapse number between a pre- and a postsynaptic population. These numbers are used for connecting the network, using the connection rule "fixed total number". (**B**) Mean number of synapses a neuron in a specific postsynaptic population is receiving from all neurons of a presynaptic population. These numbers are only applied when using the connection rule "fixed indegree".

ron k times out of C_{ab}, the total probabilities of receiving k synapses from population a is given by

$$\Pr_{\text{Binom}}\left\{X = k; n = C_{ab}, p = \frac{1}{N_b}\right\} = \binom{C_{ab}}{k}\left(\frac{1}{N_b}\right)^k\left(1-\frac{1}{N_b}\right)^{C_{ab}-k}. \tag{14}$$

Accordingly, the expected value of k is $E[k] = C_{ab}/N_b$, its variance is $\text{Var}(k) = C_{ab}(1-1/N_b)/N_b$. In Figure 3, the actual distribution of synapse numbers for the connection L6e $\rightarrow$ L6i is shown in a normalized histogram. The measured mean and standard deviation are (975 ± 31) compared to the theoretical value of (979 ± 31) synapses. Thus, the agreement between the numbers from the simulation and the theoretical expectation is in full agreement.

To further validate the model on a basic level, we take a look at a single neurons' membrane potentials Figure 4 shows

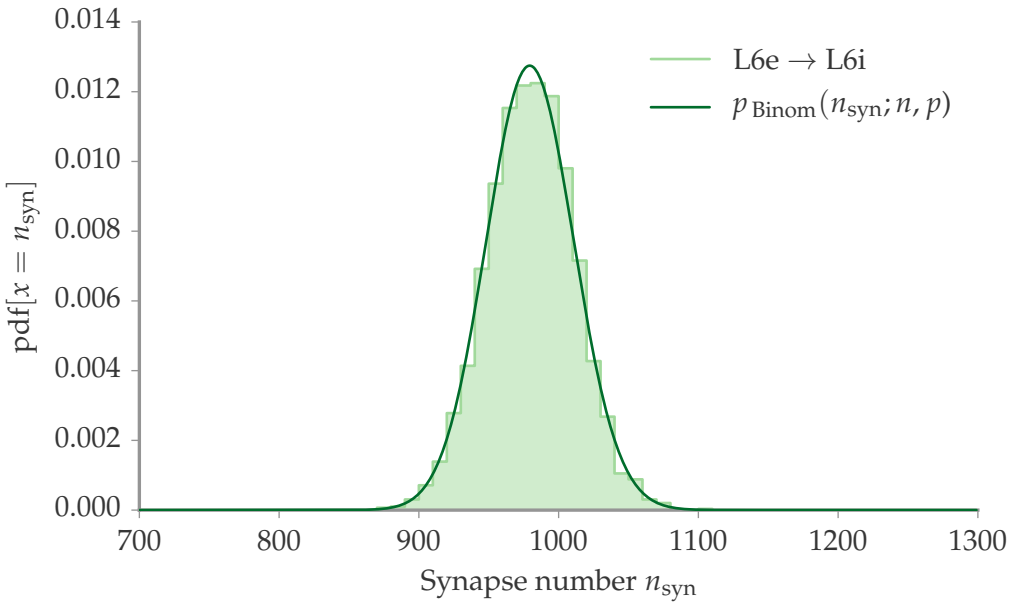

Figure 3: Distribution of synapse numbers for the connection L6e → L6i. The total number of synapses for this connection is 2,888,426, the mean number for each neuron in L6i is 979. The normalized histogram (bin width = 10) obtained from a simulation, the full line is a binomial distribution.

the membrane potentials of two neurons over the first 1.2 s of simulation together with a comparison of the normalized histograms of a larger subset of the respective population. The neuron of the upper plots appertains to the population L6e, the other one to population L6i. Observing the first 100 ms of the membrane potential indicates that the used initialization leads to a large hyperpolarization at least in these two sample neurons. Thus, for the further analysis, a transient period of 0.2 seconds is cut off the data before further analysis. For the remaining time, the membrane potentials fluctuate in a reasonable range with mean between resting potential $E_L = -65$ mV and threshold $\theta = -50$ mV, hitting the threshold as small number of times. Potjans and Diesmann [24] state that these two populations have comparably low / high rates, the excitatory one firing at ~ 1 Hz, the inhibitory one at ~ 7 Hz [24], but linking this to the membrane potential distribution can be very misleading: Rare but large fluctuations can lead to high number of spikes without substantially raising the average. Furthermore, it is can be seen, that a single neurons' membrane potential is not necessarily distributed as the population mean. This is

due to the large variation in single neuron firing rates reported already in the original publication [24].

Table 1: Model description according to Nordlie et al. [23]. Specific parameters are shown in Table 2.

MODEL SUMMARY	
Populations	8 cortical populations
Topology	–
Connectivity	Random connections with fixed number of synapses for each combination of pre- and postsynaptic population
Neuron model	Leaky integrate-and-fire, fixed voltage threshold, fixed absolute refractory period
Synapse model	Exponential-shaped postsynaptic current
Plasticity	–
Input	Independent fixed-rate Poisson spike trains to iaf neurons
Measurements	Spike activity, membrane potentials
POPULATIONS	
Layers	L2/3, L4, L5, L6
Composed of	One excitatory (e) and one inhibitory (i) population per layer
Size	Population specific size
CONNECTIVITY	
Type	Random connectivity with independently chosen pre- and postsynaptic neurons; fixed total number of connections between two populations
Weights	Fixed; drawn from clipped Gaussian distributions ($w > 0$ for excitatory, $w < 0$ for inhibitory)
Delays	Fixed; drawn from clipped Gaussian distributions ($d > 0$); multiples of computation step size
NEURONS AND SYNAPSE MODEL	
Name	iaf neuron
Type	Leaky integrate-and-fire, exponential-shaped current inputs
Subthreshold dynamics of neuron i	$\tau_m \dot{V}_i(t) = -(V_i(t) - E_L) + \frac{\tau_m}{C_m} I_i(t) \quad \text{if} \quad t > t^* + \tau_{rp}$ $V_i(t) = V_r \quad \text{else}$ $I_{syn,ij}(t) = w_{ij} \exp\left(\frac{-t}{\tau_{syn}}\right)$
Spiking	If $V_i(t_-) < \theta \quad \wedge \quad V_i(t_+) \geqslant \theta$: 1. set $t^* = t$ 2. emit spike with time stamp t^*

Table 2: Network parameters

POPULATIONS AND INPUT								
Layer	L2/3		L4		L5		L6	
Population	e	i	e	i	e	i	e	i
Pop. size, N_a	20683	5834	21915	5479	4850	1065	14395	2948
$(C_{ext})_a$	1600	1500	2100	1900	2000	1900	2900	2100
Backgr. rate	8 Hz							
CONNECTION PROBABILITIES FOR PRE- AND POSTSYNAPTIC POPULATIONS								
pre / post	L2/3		L4		L5		L6	
	e	i	e	i	e	i	e	i
L2/3e	0.101	0.169	0.044	0.082	0.032	0	0.008	0
L2/3i	0.135	0.137	0.032	0.051	0.075	0	0.004	0
L4e	0.008	0.006	0.050	0.135	0.007	0	0.045	0
L4i	0.069	0.003	0.079	0.160	0.003	0	0.106	0
L5e	0.100	0.062	0.051	0.006	0.083	0.373	0.020	0
L5i	0.055	0.027	0.026	0.002	0.060	0.316	0.009	0
L6e	0.016	0.007	0.021	0.017	0.057	0.020	0.040	0.225
L6i	0.036	0.001	0.003	0.001	0.028	0.008	0.066	0.144
FURTHER CONNECTIVITY								
$w \pm \delta w$	87.8 ± 8.8 pA		Excitatory synaptic strengths					
j_{02}	2		Factor for connection L4e → L2/3e					
g	4		Relative inhibitory synapse strength					
$d_e \pm \delta d_e$	1.5 ± 0.75 ms		Excitatory synaptic transmission delays					
$d_i \pm \delta d_i$	0.8 ± 0.4 ms		Inhibitory synaptic transmission delays					
NEURON MODEL								
τ_m	10 ms		Membrane time constant					
τ_{ref}	2 ms		Absolute refractory period					
τ_{syn}	0.5 ms		Postsynaptic current time constant					
C_m	250 pF		Membrane capacity					
E_L	−65 mV		Leaky rest potential					
V_r	−65 mV		Reset potential					
θ	−50 mV		Fixed firing threshold					

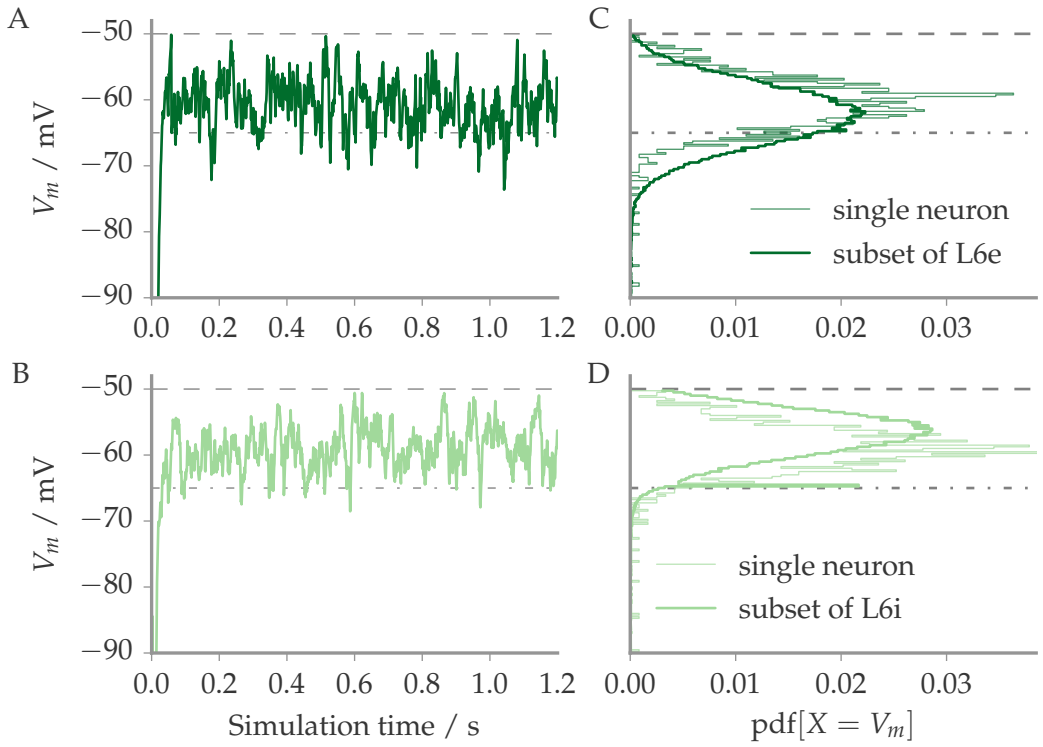

Figure 4: Membrane potentials V_m of two exemplary neurons of the populations L6e (**A, C**) and L6i (**B, D**). The data is taken from a simulation of 1.2 s, recording the membrane potential every 1 ms. For the histograms, the first 0.2 s are discarded. In all four plots, the threshold $\theta = -50$ mV is indicated by a dashed line, the resting potential $E_L = -65$ mV by a line of dashes and dots. (**A, B**) Membrane potential over the time of simulation. The upper membrane potential reaches θ once at $t = 0.06$ s, the lower one does not spike over the time recorded. The initial membrane potential is drawn from a normal distribution. (**C, D**) Normalized histograms of membrane potentials of the two neurons (thin steps) as well as the averaged ones for a subset of 100 neurons (thick steps). Note that contributions due to neurons being in refractory period after spiking are not removed, yielding peaks at $V_r = -65$ mV.

2.2 MEAN FIELD MODEL

THE DERIVATION of a mean field theory goes along the lines of the work by Brunel [8]. It starts of with a simplified model of N leaky integrate-and-fire neurons in two populations. Each neuron receives input from the network by C synapses, C_E from excitatory and C_I from inhibitory ones. Furthermore, each neurons receives $C_{ext} = C_E$ connections from external excitatory neurons. The synapse numbers are determined by the relative size of the two populations through the factor

$$\epsilon := \frac{C_E}{N_E} = \frac{C_I}{N_I} \,. \tag{15}$$

A central assumption is the sparsity of the network, expressed by $\epsilon \ll 1$. Guided by anatomical estimates for the neocortex, the population sizes are set to $N_e = 0.8N$ excitatory and $N_i = 0.2N$ inhibitory neurons. Taking equation (15), this implies

$$C_I = \gamma C_E \tag{16}$$

with $\gamma = 0.25$. The synaptic weights in this model are set to J for excitatory presynaptic neurons and to $-g\,J$ for inhibitory ones, whereas the delays are fixed to d for all synapses.

At the heart of the mean field model is the transition from the deterministic description of membrane potential dynamics to a probabilistic formulation. As in the spiking network model of the last section, the membrane potential follows the differential equation (2) of the leaky integrate-and-fire neuron. The input is simplified by implementing voltage based synapses which yield an instantaneous and fixed voltage change for each spike arriving at the neuron, so-called δ-synapses: The change in membrane potential of a neuron i due to all incoming spikes fired by neurons j at time t_j^k can be described by a sum over Dirac delta-functions,

$$R\,I_i(t) = \tau_m \sum_j J_{ij} \sum_k \delta(t - t_j^k - d_{ij}) \,. \tag{17}$$

The synaptic weights J_{ij} is in this case given in mV; d_{ij} is the delay between neuron i and j. Note that the membrane capacitance is included in the resistance $R = \tau_m / C_m$.

Two important conditions have to be met in order to make the transition from this description to a probabilistic one:

- Sparsity: This implies that two neurons share only a small number of common input, such that pair correlations are negligible for $C/N \to 0$;

- Uncorrelated input: The contributions a neuron receives have to stem from a wide range of the network, each being small compared to the threshold (corresponding to negligible spatial correlations). No temporal correlations imply low single neuron firing rates ν compared to the membrane time constant τ_m (e. g. $\nu \sim 10$ Hz and $1/\tau_m \sim 1/(20\,\text{ms}) = 50\,\text{Hz}$).

If these conditions are met, the input can be modeled as a time-varying average part $\mu(t)$ plus a fluctuating Gaussian part with variance $\sigma(t)\tau_m$:

$$\frac{\tau_m}{C_m} I_i(t) = \mu(t) + \sigma(t)\sqrt{\tau_m}\eta_i(t)\,. \tag{18}$$

The random fluctuations are described by Gaussian white noise $\eta_i(t)$ with $\langle \eta_i(t) \rangle = 0$ and unit variance. The exclusion of correlations is formalized as

$$\langle \eta_i(t)\,\eta_j(t') \rangle = \delta_{ij}\,\delta(t-t')\,, \tag{19}$$

δ_{ij} corresponding to correlations between neurons, the Dirac delta distribution to temporal ones.

The fundamental parameter calculated by the mean field model is the single neuron firing rate $\nu(t)$. In this basic model, it is assumed that any neuron of either of the two populations sees the same input on average and thus fires with the same rate ν. This rate is linked to the average input $\mu(t)$ by

$$\begin{aligned} & \mu(t) = \mu_l(t) + \mu_{ext} \\ \text{with} \quad & \mu_l(t) = C_E\,J(1-\gamma g)\nu(t-d)\tau_m \\ \text{and} \quad & \mu_{ext} = C_E J \nu_{ext}\tau_m\,. \end{aligned} \tag{20}$$

The tow summands correspond to the local (i. e. recurrent) and external input, respectively. Similarly, for the amplitude of fluctuations $\sigma(t)$:

$$\begin{aligned} & \sigma^2(t) = {\sigma_l}^2(t) + {\sigma_{ext}}^2 \\ \text{with} \quad & {\sigma_l}^2(t) = C_E\,J^2(1+\gamma g^2)\nu(t-d)\tau_m \\ \text{and} \quad & {\sigma_{ext}}^2 = C_E J^2 \nu_{ext}\tau_m\,. \end{aligned} \tag{21}$$

These quantities can also be related to measures in a simulation: If one takes a single neuron together with the spike trains of all its presynaptic neurons, entering the spike times in the corresponding equation for the input (e. g. equation (3) in case of the spiking network introduced before) yields the actual input

over time. Empirical mean and variance can then be directly compared to μ and $\sigma^2\tau_m$.

Brunel then transforms equations (18) and (2) into a Fokker–Planck equation describing the probability distribution of the membrane potential $P(V,t)$ in time:

$$\tau_m \frac{\partial P(V,t)}{\partial t} = \frac{\sigma^2(t)}{2} \frac{\partial^2 P(V,t)}{\partial V^2} + \frac{\partial}{\partial V}[(V-\mu(t))P(V,t)]\,. \quad (22)$$

In the terminology of stochastic differential equations, the first term on the right hand side corresponds to a diffusion term originating in the fluctuations σ of the input whereas the second part describes a drift due to the respective mean μ and the leaky quality of the neuron model. Introducing the probability current

$$S(V,t) = -\frac{\sigma^2(t)}{2\tau_m}\frac{\partial P(V,t)}{\partial V} - \frac{V-\mu(t)}{\tau_m}P(V,t) \quad (23)$$

through V at time t yields the continuity equation

$$\frac{\partial P(V,t)}{\partial t} = -\frac{\partial S(V,t)}{\partial V}\,. \quad (24)$$

The probability distribution is subject to a number of constraints: Since the spiking resets neurons to $V_{rp} < \theta$, the membrane potential is always below this threshold: $P(V,t) = 0$ for $V > \theta$. Infinite probability currents are excluded such that $P(V,t)$ must be continuous at any point. Specifically, this continuity forbids infinite spiking probabilities at the threshold θ. The resulting constraint is

$$P(\theta,t) = 0\,. \quad (25)$$

The probability current at the threshold is equal to the firing rate $\nu(t)$. Inserting both $S(\theta,t) = \nu(t)$ and the above constraint into equation (23) yields

$$\frac{\partial P(\theta,t)}{\partial V} = -\frac{2\nu(t)\tau_m}{\sigma^2(t)}\,. \quad (26)$$

Neurons that fired at time t exit their refractory period at time $t+\tau_{rp}$ at the reset potential V_r. This leads to a difference in probability current below and above V_r proportional to the rate of neurons firing at $t-\tau_{rp}$, which is expressed by

$$\frac{\partial P(V_r^+,t)}{\partial V} - \frac{\partial P(V_r^-,t)}{\partial V} = -\frac{2\nu(t-\tau_{rp})\tau_m}{\sigma^2(t)}\,. \quad (27)$$

Finally, $P(V,t)$ is assumed to converge sufficiently quickly to zero:

$$\lim_{V\to-\infty} P(V,t) = 0\,; \quad \lim_{V\to-\infty} VP(V,t) = 0\,. \tag{28}$$

A stationary solution $P(V,t) = P_0(V)$ with constant single neuron firing rate ν_0 satisfying the above boundary conditions is then given by:

$$P_0(V) = 2\frac{\nu_0\tau_m}{\sigma_0}\exp\left(-\frac{(V-\mu_0)^2}{{\sigma_0}^2}\right)\int_{\frac{V-\mu_0}{\sigma_0}}^{\frac{\theta-\mu_0}{\sigma_0}}\Theta\left(u-\frac{V_r-\mu_0}{\sigma_0}\right)e^{u^2}\,du\,. \tag{29}$$

Here, $\Theta(x)$ is the Heaviside step function, i. e.

$$\Theta(x) = \begin{cases} 1 & \text{if } x \leqslant 0 \\ 0 & \text{else} \end{cases}\,. \tag{30}$$

The stationary mean input and fluctuation amplitudes are obtained by inserting ν_0 into the equations (20) and (21), yielding

$$\mu_0 = C_E J\,\tau_m[\nu_{ext} + \nu_0(1-g\gamma)]\,, \tag{31}$$
$${\sigma_0}^2 = C_E J^2\,\tau_m[\nu_{ext} + \nu_0(1+g^2\gamma)]\,. \tag{32}$$

To interpret $P(V,t)$ as a probability distribution, it is required to satisfy the normalization condition

$$\int_{-\infty}^{\theta} P(V,t)\,dV + p_r(t) = 1\,, \tag{33}$$

where

$$p_r(t) := \int_{t-\tau_{rp}}^{t} \nu(u)\,du \tag{34}$$

is the probability of neurons being the in refractory period. In the constant case, this is simply

$$p_r(t) = p_{r,0} = \nu_0\tau_{rp}\,. \tag{35}$$

Inserting both $P_0(V)$ and $p_{r,0}$ into the self-consistent condition (33) then leads to an expression for ν_0:

$$\begin{aligned}
\frac{1}{\nu_0} &= \tau_{rp} + \frac{1}{\nu_0}\int_{-\infty}^{\theta} P_0(V)\,dV \\
&= \tau_{rp} + \frac{2\tau_m}{\sigma_0}\int_{-\infty}^{\theta}\left[\exp\left(-\frac{(V-\mu_0)^2}{{\sigma_0}^2}\right)\int_{\frac{V-\mu_0}{\sigma_0}}^{\frac{\theta-\mu_0}{\sigma_0}}\Theta\left(u-\frac{V_r-\mu_0}{\sigma_0}\right)e^{u^2}\,du\right]dV \\
&= \tau_{rp} + \frac{2\tau_m}{\sigma_0}\int_{\frac{V_r-\mu_0}{\sigma_0}}^{\frac{\theta-\mu_0}{\sigma_0}}\left[e^{u^2}\int_{-\infty}^{u\sigma_0+\mu_0}\exp\left(-\frac{(V-\mu_0)^2}{{\sigma_0}^2}\right)dV\right]du \\
&= \tau_{rp} + 2\tau_m\int_{\frac{V_r-\mu_0}{\sigma_0}}^{\frac{\theta-\mu_0}{\sigma_0}}\left[e^{u^2}\int_{-\infty}^{u}e^{v^2}\,dv\right]du \\
&= \tau_{rp} + \tau_m\sqrt{\pi}\int_{\frac{V_r-\mu_0}{\sigma_0}}^{\frac{\theta-\mu_0}{\sigma_0}} e^{u^2}\,(1+\mathrm{erf}(u))\,du\,,
\end{aligned} \tag{36}$$

where erf is the error function. As done by Brunel [8], this equation can be solved numerically for varying parameters to characterize the different states the system can be found in.

WHAT HAS BEEN INTRODUCED so far serves as a basis for the theory newly derived for this thesis. In order to transfer results to the model of the neocortical microcircuit, the contributions to the input have to be adapted for each population. Instead of parametrized μ_0 and σ_0 in terms of the variables C_E, J, g and γ, a matrix notation as in equation (1) is utilized: Synapse numbers and weights are defined as C_{ab} and J_{ab}, respectively, where a is the postsynaptic and b the presynaptic population. Finally, the external input is written in a similar notation: An external excitatory population with single neuron firing rate ν_{ext} is connected to a neuron in population a by $(C_{ext})_a$ synapses. Since all external populations in this study are excitatory and we do not include dependence on the postsynaptic neuron, the corresponding weight is simply J. Including these definitions, we can write the mean input and fluctuation amplitude as

$$\mu_a = \tau_m \sum_{b\,\in\,\mathrm{pop.}} C_{ab}\,J_{ab}\,\nu_b + \tau_m (C_{ext})_a\,J\,\nu_{ext}\,; \tag{37}$$

$${\sigma_a}^2 = \tau_m \sum_{b\,\in\,\mathrm{pop.}} C_{ab}\,{J_{ab}}^2\,\nu_b + \tau_m (C_{ext})_a\,J^2\,\nu_{ext}\,, \tag{38}$$

where the sums go over all internal populations. μ_a and σ_a can be further adjusted to match the parameters of the spiking network model. One such adaption is to include the variance of the synaptic weight distribution following the early work of Amit and Brunel [3]. If the synaptic weights between pre- and postsynaptic population a and b are drawn from a normal distribution with mean J_{ab} and relative standard deviation $\Delta_{J,ab}$, then the additional variance of the input is independent of the structural and temporal one of equation (38) and can simply be added. Thus, the factor entering equation (38) is ${J_{ab}}^2 + (\Delta_{J,ab} J_{ab})^2$ and analogously for the external part. Using the same relative standard deviation Δ_J for all recurrent and external synapses, we simply multiply the right hand side of equation (38) by the factor $(1 + {\Delta_J}^2)$.

A further adjustment takes into account that the synapse type used in simulation does not deliver the applied voltage immediately. Although the synaptic weight w_{ab} of the current based synapses in the spiking network model is obtained using the experimentally accessible peak PSP (as described in Methods, Section 2.1), the effective change in membrane potential in the mean field model is not equal to the peak PSP. Instead, an effective synapse strength for the mean field model can be obtained by matching the two synapse types. The procedure is based on one pursued by Sadeh et al. [30] for the case of α-synapses, and adopted here for the applied exponential synapses. The incoming current due to a spike entering the synapse at time $t = 0$ is defined by the model of neuron and synapse. For the spiking network model, the equations (2) and (3), the corresponding term is

$$RI_e(t) = \frac{\tau_m}{C_m} w \, e^{\frac{t}{\tau_m}}, \tag{39}$$

a while for the mean field model a single spike corresponds to one Dirac delta-function,

$$RI_\delta(t) = \tau_m J \, \delta(t), \tag{40}$$

compare to equation (17). Note that eq. (39) is also written in voltage units for comparability. The kernels of the two synapse models are $k_e(t) = e^{\frac{t}{\tau_m}}$ and $\delta(t)$, respectively. The idea is now to normalize the exponential kernel by matching its integral to the one of the δ-kernel:

$$\int_0^\infty \delta(t)\, dt = 1 = a_\mu \int_0^\infty k_e(t)\, dt = a_\mu \tau_s, \tag{41}$$

introducing the normalization factor $a_\mu = 1/\tau_s$. In a second step, we exchange the δ-kernel of equation (40) with the normalized one and match this combination with the actual exponential synapse, integrating over the entire domain:

$$\int_0^\infty \tau_m \, J \, a_\mu \, k_e(t) \, dt = \int_0^\infty \frac{\tau_m}{C_m} \, w \, k_e(t) \, dt \,, \tag{42}$$

which yields

$$J = \frac{w \, \tau_s}{C_m} \,. \tag{43}$$

This is the synapse weight factor applied in the model. Th magnitude of the variance ${\sigma_a}^2$, however, is not captured by J^2. Hence, we introduce the effective factor ${J_{eff}}^2$ and obtain it by an analogue procedure. In this case, the square of the kernel $k_e(t)$ is normalized:

$$\begin{aligned} 1 &= {a_\sigma}^2 \int_0^\infty (k_e(t))^2 \, dt \\ &= {a_\sigma}^2 \int_0^\infty e^{\frac{-2t}{\tau_s}} \, dt \\ &= {a_\sigma}^2 \, \frac{\tau_s}{2} \,, \end{aligned} \tag{44}$$

which sets the normalization factor to ${a_\sigma}^2 = 2/\tau_s$. Inserting as before but squaring both sides under the integral yields

$$\int_0^\infty (\tau_m \, J \, a_\sigma \, k_e(t))^2 \, dt = \int_0^\infty \left(\frac{\tau_m}{C_m} \, w \, k_e(t) \right)^2 dt \,, \tag{45}$$

which results in

$${J_{eff}}^2 = \frac{w^2}{{C_m}^2} \, \frac{\tau_s}{2} \,. \tag{46}$$

Note that this is in agreement with the units chosen: We have

$$[J] = \left[\frac{w \tau_s}{C_m} \right] = V \tag{47}$$

$$\text{and} \quad \left[{J_{eff}}^2 \right] = \left[\frac{w^2 \tau_s}{{C_m}^2} \right] = \frac{V^2}{s} \,, \tag{48}$$

using the relationship between voltage, current and capacitance, $V = [R \cdot I] = [t/C] \cdot [I]$. This finally agrees with $[\mu^2] = [\sigma^2 \cdot t]$ (cf. equation (18)) since

$$[\mu] = [\tau_m J \nu] = V \tag{49}$$

$$\text{and} \quad [\sigma^2] = [\tau_m {J_{eff}}^2 \nu] = V^2/s \,. \tag{50}$$

Including both the variance of the synaptic weights as well as the adaption for the synapse type, we can conveniently write the average input μ_a and variance ${\sigma_a}^2$ introducing the quantities

$$(M_{\text{local}})_{ab} := \tau_m \, C_{ab} \, J_{ab} \, ; \tag{51}$$

$$(M_{\text{ext}})_a := \tau_m \, (C_{\text{ext}})_a \, J \, ; \tag{52}$$

$$(S_{\text{local}})_{ab} := \tau_m \, (1 + {\Delta_J}^2) \, C_{ab} \, ({J_{\text{eff}}}^2)_{ab} \, ; \tag{53}$$

$$(S_{\text{ext}})_a := \tau_m \, (1 + {\Delta_J}^2) \, (C_{\text{ext}})_a \, {J_{\text{eff}}}^2 \tag{54}$$

for local and external input. $({J_{\text{eff}}}^2)_{ab}$ is obtained by inserting the mean weights for populations a and b in equation (46). The extended equations (37) and (38) then read

$$\mu_a = \sum_{b \in \text{pop.}} (M_{\text{local}})_{ab} \, \nu_b + (M_{\text{ext}})_a \, \nu_{\text{ext}} \, ; \tag{55}$$

$${\sigma_a}^2 = \sum_{b \in \text{pop.}} (S_{\text{local}})_{ab} \, \nu_b + (S_{\text{ext}})_a \, \nu_{\text{ext}} \, . \tag{56}$$

With these parameters, we turn back to the self-consistency condition (36). Extending the model yields eight equations for the firing rate ν_a of neurons in population a,

$$\frac{1}{\nu_a} = \tau_{\text{rp}} + \tau_m \sqrt{\pi} \int_{\frac{V_r - \mu_a}{\sigma_a}}^{\frac{\theta - \mu_a}{\sigma_a}} e^{u^2} \, (1 + \operatorname{erf}(u)) \, du \, . \tag{57}$$

These equations are coupled by the boundaries of the integrals. Note that the index 0 is omitted to facilitate readability, as the results are only concerned with stationary solutions. After the rates ν_a are found, these values can be plugged into an equation for the distribution of membrane potentials. Extending the corresponding expression (29) to more populations and again dropping the index 0 yields

$$P_a(V) = 2 \frac{\nu_a \tau_m}{\sigma_a} \exp\left(- \frac{(V - \mu_a)^2}{{\sigma_a}^2} \right) \int_{\frac{V - \mu_a}{\sigma_a}}^{\frac{\theta - \mu_a}{\sigma_a}} \Theta\left(u - \frac{V_r - \mu_a}{\sigma_a} \right) e^{u^2} \, du \, . \tag{58}$$

In a reasonable regime, this function can be approximated by a Gaussian curve and an additional discontinuity in the first derivative at V_r (a visible "kink" or "step"). Ultimately, the model also makes a prediction about the regularity of single spike trains. For neurons firing irregularly, the interspike intervals

(ISI, i. e. the difference in times between two successive spikes of one neuron) are distributed broadly. Hence, one parameter to measure irregularity is the coefficient of variation (CV) of ISI, defined as

$$\mathrm{CV}_{\mathrm{ISI}} = \frac{\sigma_{\mathrm{ISI}}}{\mu_{\mathrm{ISI}}}\,. \tag{59}$$

Here, σ_{ISI} and μ_{ISI} are the standard deviation and mean of the ISI. This quantity can be calculated independently for each population. For the given parameters ν_a, μ_a and σ_a as in equation (57), the corresponding result of Brunel [8] is

$$\mathrm{CV}_{\mathrm{ISI}}^2 = 2\pi \left(\frac{\nu_a}{\tau_m}\right)^2 \int_{\frac{V_r-\mu_a}{\sigma_a}}^{\frac{\theta-\mu_a}{\sigma_a}} e^{x^2}\,dx \int_{-\infty}^{x} e^{u^2}\,(1+\mathrm{erf}(u))^2\,du\,. \tag{60}$$

The CV of ISI is also an experimentally accessible quantity. An example for observed values in neocortical neurons is given by Nawrot et al. [21], who report values of $\mathrm{CV}_{\mathrm{ISI}} \sim 0.4 - 0.6$ in a task-related monkey experiment recording from single neurons of the primary visual cortex.

2.3 IMPLEMENTATION AND ANALYSIS

THE SIMULATIONS are implemented with the NEST simulation tool using its Python interface PyNEST [13]. The differential equations of the network are solved with a computational step size of $h = 0.1$, applying a numerical method known as "exact integration" [28]. Numerical solution as well as the analysis of the data is done in using python [27] and heavily relies upon the NumPy–SciPy framework [18]. Plots are created using Matplotlib [17]. The source code both for simulation and analysis can be reviewed at my GitHub repository [1] or more conveniently with the IPython Notebook Viewer [2].

The analysis of the data obtained from simulations contains a number of statistical measures. The data is taken from randomly chosen subsets of each population, containing 1000 neurons for spikes, 100 in the case of membrane potentials. The single neuron firing rate ν_{sim} is obtained dividing the number of spikes by the time simulated. For a measure of irregularity of spike trains, the times difference between two successive spikes (the ISI) for all neurons that fired more than two times are taken. Dividing the standard deviation of ISI by its mean yields the corresponding quantity, the empiric CV of ISI. Both firing rate

and CV of ISI are then averaged over the recorded subpopulation. Measuring the synchrony of neurons within a population is achieved by calculating a histogram of the spike times of the entire subpopulation with fixed bin width of 3 ms (referred to as peristimulus time histogram, PSTH). The synchrony is then defined by calculating the Fano factor (13) of the PSTH. A theoretical prediction in the framework of the mean field theory is not calculated. However, to get a reference point, one can calculated the synchrony of an ensemble of uncorrelated Poisson processes, corresponding to the case of asynchrony. Since the individual processes are uncorrelated, mean and variance of the sum of spike trains are equal to the sum of the single processes' means and variances. Since for each process, mean and variance are equal, the resulting synchrony measure is 1. The spiking of single neurons in the mean field model can be described as a renewal process: The probability of spiking only depends on the last spike time, memory about further past is lost at spiking. For this class of stochastic processes, the Fano factor of a single neuron's spike train (and thus the synchrony measure for uncorrelated spike trains) can be computed using the higher moments of the ISI distribution (see e. g. van Vreeswijk [33] for an overview). In principle, this can be done for the given process, but this extension lies outside the scope of this thesis. The given approximation of the Fano factor by the CV of ISI [33] is only valid for large time bins compared to the inverse firing rate – a regime far from that of the mean field model (bin width of 3 ms and inverse of rate $\sim$ 5 Hz).

The evaluation of membrane potentials of simulated neurons requires a specific treatment for neurons residing in refractory period at the $V_r = -65$ mV. Since the membrane potential predicted by the mean field theory does not include those neurons, the respective fraction for the measured ones has to be taken out. This is done as follows: Each neuron i of population a with firing rate $\nu_{a,i}$ measured over a recording time T spends a time of $T\tau_{rp}\,\nu_{a,i}$ in refractory period. If T is divided into n_T time bins, this corresponds to $n_T\,\tau_{rp}\,\nu_{a,i}$ time bins. The total number of entries corresponding to neurons in refractory period $n_{tot,rp,a}$ is then calculated by summing over all neurons, i. e.

$$n_{tot,rp,a} = n_T\,\tau_{rp} \sum_{i=1}^{n_{rec}} \nu_{a,i}\,. \tag{61}$$

This number is subtracted from the bin at $V_m = E_L$. Normalization of the histogram less neurons in refractory period is then achieved dividing the frequencies by the factor $n_T\, n_{rec}\, \Delta V_m$, with the bin widths ΔV_m of the voltage histogram.

The resulting integrals of the mean field theory, appearing in the equations (57), (58) and (60), are solved numerically. Because of limited precision, special care has to be taken in the case of the error function erf(u): While for the analytical function $|\mathrm{erf}(u)| < 1$ on the entire domain $u \in \mathbb{R}$, the numerical evaluation of $\mathrm{erf}(\pm u)$ yields exactly ± 1.0 for large values $u > 0$. For negative values of u, the factor $(1 + \mathrm{erf}(u))$ thus becomes zero. In order to avoid this arithmetic underflow, the scaled complementary error function

$$\mathrm{erfcx}(u) := e^{u^2}(1 - \mathrm{erf}(u)) \tag{62}$$

is applied. That is,

$$e^{u^2}\,(1 + \mathrm{erf}(u)) = \mathrm{erfcx}(-u) \tag{63}$$

and

$$e^{u^2}\,(1 + \mathrm{erf}(u))^2 = e^{-u^2}\mathrm{erfcx}(-u)^2 \tag{64}$$

for the integrands of the self-consistency equation (57) and the CV of ISI, (60), respectively.

A solution to equation (57) is not necessarily found for any initial guess. To achieve convergence, two possibilities can be applied: In the case of rates known from simulation, these serve as an initial guess. A test with simulated rates from 20 independent simulations for 20 seconds each lead to convergence[3] most after a number of 42 ± 12 steps (mean and standard deviation). The second solution entirely independent of simulation data is solving the simpler model with only two populations corresponding to equation (36), first. The model can then be split into eight populations and all parameters can be iteratively transformed to the ones of the model in question.

3 Convergence is here defined by a maximum relative distance $\|\nu_{i+1} - \nu_i\|/\|\nu_i\| \leqslant 10^{-13}$ between two successively computed vectors ν_i with entries $\nu_{i,a}$ [18]

3 RESULTS

3.1 SPIKING NETWORK MODEL

THE SPIKING NETWORK MODEL will be analyzed in the following manner: At first, the results are directly compared to those obtained by the original model of Potjans and Diesmann. Both simulations are run for the same parameters, differences arise solely due to internal differences in assigning the random number generators. It is therefor not feasible to do a direct (spike per spike) comparison. Instead, a statistical description is chosen which furthermore sheds light on the differences between individual realizations with different seeds for the random number generators. The distribution of single neuron firing rate within the population and the interspike interval distributions. are then analyzed more thoroughly.

A comparison between the PyNEST implementation and the original one written in SLI is supplied in form of raster plots (Figure 5), showing the activity of a subset of the network simulated for 400 ms after a transient period of 200 ms. The subset shown consists of the first 2.5 % of the neurons of each population created during the initialization of the network. Both results have a very similar structure: The corresponding subsets show about the same number of events per time. This number varies strongly between different populations. Specifically, populations L2/3e and L6e fire at much lower frequencies compared to the remaining populations. Furthermore, both simulations show some signs of synchrony within populations, indicated by spikes of different neurons aligned in vertical lines. This is most apparent for the populations L2/3e, L2/3i, L4e and L5e.

A more thorough comparison is done on the bases of three statistical quantities: Figure 6 shows the population means of single neurons firing rates, irregularity as measured by the CV of ISI as well as a measure for synchrony (the Fano factor of the PSTH) for both simulations (see Methods, Section 2.3 for details). All parameters were calculated from 20 repetitions of a simulation for 60 s. Spikes were recorded from 1000 neurons of each population, with recording starting after a transient period

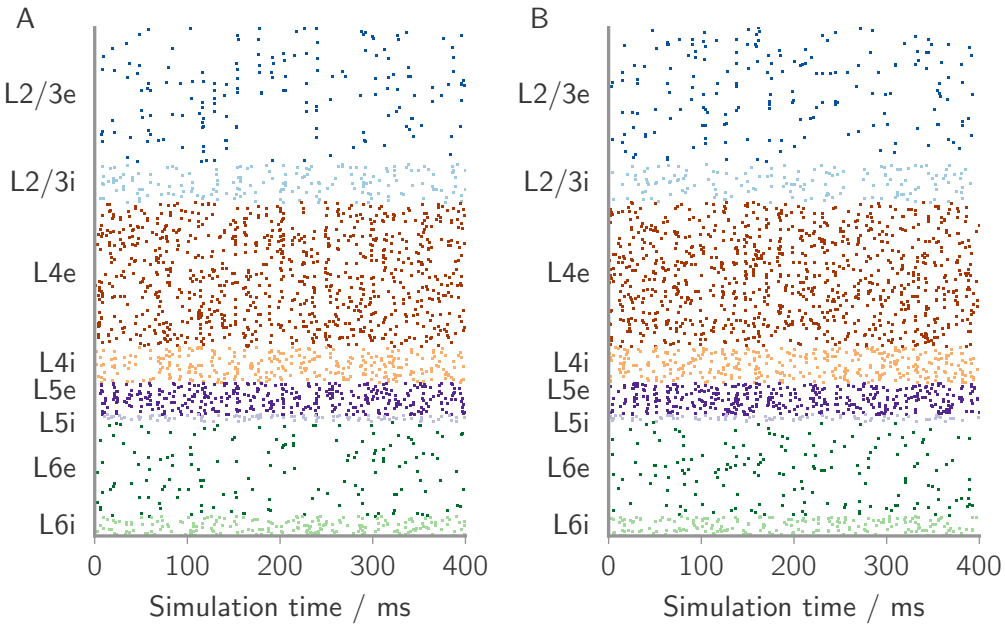

Figure 5: Raster plot showing spontaneous activity of network for (A) the PyNEST implementation and (B) the SLI implementation. The simulation and network parameters for both simulations are the same. For each layer, the excitatory population is the upper one shown (total of 1924 neurons) for 400 ms.

of 0.2 s. For all three quantities, both implementations are in full agreement for the statistical fluctuations observed. Fluctuations between different initializations differ for each quantities: For the firing rates, the largest variance is observed for L5e. For the irregularity, fluctuations are much smaller with the highest ones seen in populations L2/3e and L6e. Finally, the variation for synchrony is largest for L2/3e and L5e. For synchrony and firing rates, there is a tendency for the fluctuations to be larger for larger values of the respective quantity – note however the exception of L5i firing rate, which shows very little fluctuation.

In order to get a deeper insight into the dynamics of the simulated network, the firing rates and the CV of ISI of single neurons are examined in Figure 7. The observed fluctuations around the population mean are remarkably large and can be tracked back to the specific connection rule applied. Note, however, that despite being large within a population, the fluctuations of the population means for different realizations remains small – an observation important for the application of a mean

field model. Both aspects will be reviewed in the Discussion, Chapter 4.

3.2 MEAN FIELD THEORY

IN THE FOLLOWING SECTION , the results of the mean field theory are presented. by showing the predicted firing rates and utilizing these rates to predict the previously introduced measure of irregularity as well as the distribution of membrane potentials. These results are directly compared to the corresponding quantities recorded from the spiking network model simulation and analyzed in the previous section. The average input μ to each neuron is examined by separating the recurrent an external contribution. Finally, the possibility of applying the mean field model as a predictive tool is illustrated by calculating firing rates for varying relative inhibitory synapse strength g and external frequency ν_{ext}.

The firing rates obtained by solving equation (57) are displayed in a bar plot in Figure 8. Rates measured in simulation and previously shown in Figure 6 are shown for comparison. As visible, the results of the mean field model match those of the simulation to a high degree:

The predicted rates cover those observed in simulation for the populations of all layers by L5. For the latter one, the rate of the excitatory population is underestimated, the inhibitory one predicted slightly too high. Qualitatively, the sequence of populations ordered by increasing firing rates is reproduced. The comparison can further be quantified: The difference $\Delta\nu_a := \nu_{mf,a} - \nu_{sim,a}$ between the mean of simulated rates $\nu_{sim,a}$ and predicted rates $\nu_{mf,a}$ for each population a is shown in Table 3. The mean and standard deviation of the absolute values of $\Delta\nu_a$ are (0.22 ± 0.16) Hz. The relative difference is largest for L2/3e with $-11\,\%$, while for all other populations the relative difference is smaller or equal $7\,\%$. The irregularity measured by the mean CV of ISI for each population is the result of plugging in the predicted rates into equation (60). As for the rates, a comparison with simulation data is shown in Figure 8, while numerical results are subsumed in Table 3, using definitions analogous to those for the rates. The theoretical results agree well: The relative difference between measured and predicted values is lower than $10\,\%$ for all populations and again the order by sorting the populations according to increasing CV of ISI is reproduced. There is, however, a systematic overestimation of irregularity

for all populations. The largest deviation is found for the populations L2/3e and L6e. For both populations, the mean field theory predicts a CV of ISI of almost one, corresponding to the case of a Poisson process.

Table 3: Difference between predicted and simulated population means for firing rates and CV of ISI; absolute and relative to simulated quantities.

POPULATION	L2/3		L4		L5		L6	
	e	i	e	i	e	i	e	i
$\nu_{mf,a}$ / Hz	0.82	3.02	4.64	6.12	7.14	8.92	1.04	8.09
$\nu_{sim,a}$ / Hz	0.92	3.00	4.40	5.84	7.70	8.65	1.10	7.84
$\Delta\nu_a$ / Hz	-0.10	0.01	0.24	0.28	-0.56	0.27	-0.06	0.24
$\Delta\nu_a/\nu_{sim,a}$	-0.11	4e-3	0.05	0.05	-0.07	0.03	-0.05	0.03
$CV_{mf,a}$	0.99	0.94	0.92	0.91	0.89	0.84	0.99	0.85
$CV_{sim,a}$	0.92	0.92	0.89	0.88	0.84	0.81	0.91	0.81
ΔCV_a	0.07	0.03	0.03	0.03	0.05	0.04	0.08	0.04
$\Delta CV_a/CV_{sim,a}$	0.07	0.03	0.03	0.04	0.06	0.05	0.08	0.05

Applying equation (58) for the predicted rates yields the membrane potential distributions shown in Figure 9. The obtained distributions are compared with the normalized histograms of recorded membrane potentials of a subpopulation of $n_{rec} = 100$ neurons for each population. The contribution due to neurons in refractory period is removed (see Methods, Section 2.3 for details). The predictions agree well with the measured data: The overall shape, width and height of the distributions are recovered. For all populations, the maxima are shifted toward the resting potential $V_r = -65$ mV. The effect of neurons coming out of refractory period is underestimated in some cases, visible for example in populations L2/3i and L4i where the mean distributions show a step while the kink in the theoretical curves is hardly detectable.

TO ILLUSTRATE the average input μ to a neuron, the summands of the local input, cf. equation (55), the total local and external input μ_{local} and μ_{ext} as well as their sum are shown in Figure 10. One observes that the recurrent input is concen-

trated mostly within layers, either on the diagonal or neighboring it. A notable exception is the input of layer 4 to neurons of layer 2/3. Summing each row yields the total local input μ_{local} per neuron for each population. It is inhibitory for each population. L6e is inhibited most strongly, which is in agreement with the low firing rate. However, this observation has only limited meaning, as both external rates as well as fluctuations are not taken into account. The external input μ_{ext} balances the recurrent one, yielding positive values for all populations. In agreement with the firing rates, population L2/3e and L6e receive very little mean input. Contrary to this, population L6i receives even slightly more than L5i (7.9 mV as opposed to 7.8 mV), while the latter one fires with a higher frequency. This shows the importance of including the fluctuations.

We can now vary specific parameters in the mean field theory and predict the network activity for the resulting new model. This is interesting, as a model used for explaining experimental data should be expected to be rather robust against changes in specific parameters. One parameter that is estimated very differently in different theoretical models is the inhibitory synaptic strength g (Sadeh et al. [30] for example uses $g = 8$). In Figure 11, the firing rates are calculated for g varying over the range from 3 to 10. A first observation is the general decrease of firing rates with increasing g. The individual populations, on the other hand, do not decrease at the same rate, such that the characteristic order of firing rates is changed. This is especially the case for population L4e, which stays almost constant on the entire range (remaining at the highest rate for very strong inhibition dominance) and L2/3e, for which the rate even increases. The strongest decrease is observed for layer L5e. Note that Potjans and Diesmann [24] apply this change in g in simulation. The data shown (Figure 8 of [24]) agrees with the predictions of the model, although comparison is limited to excitatory populations. For g lower than 3, the applied algorithm does not find a solution any more. For very low inhibition, however, the mean field model's assumptions are not necessarily met any more, since individual firing rates tend to rise.

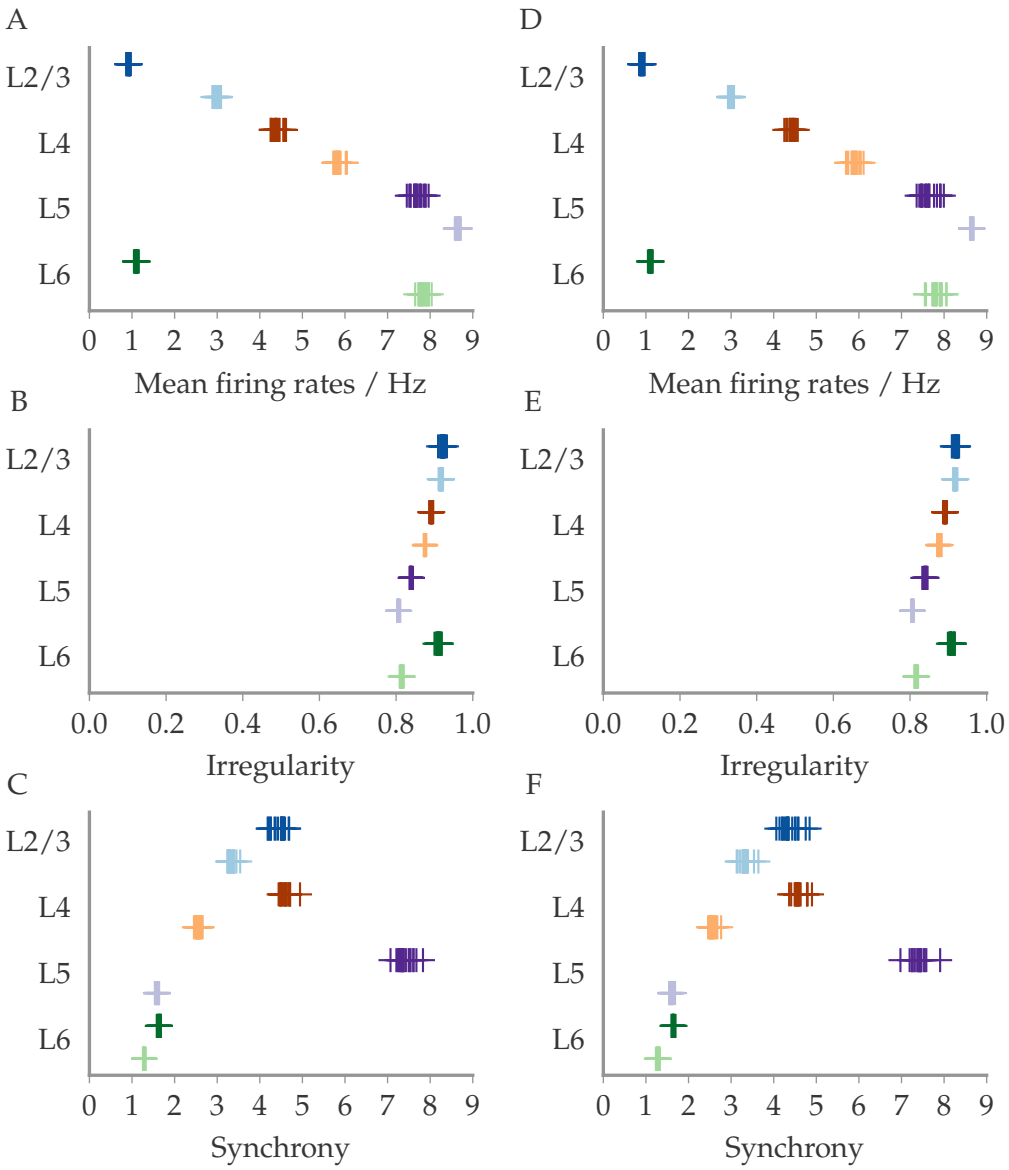

Figure 6: Measures of spontaneous activity for (**A - C**) the PyNEST implementation and (**D - E**) the SLI implementation, using the same simulation and network parameters. Both implementations are run 20 times independently (one marker per simulation), measuring 1000 spike trains of each population in a simulation for 60 s. In case of small fluctuations, individual markers may not be identified due to overlap. (**A, D**) Population mean of single neuron firing rates. (**B, E**) Irregularity of spike trains measured by the population mean of CV of ISI. (**C, F**) Synchrony of populations quantified by the Fano factor of the PSTH (bin width 3 ms).

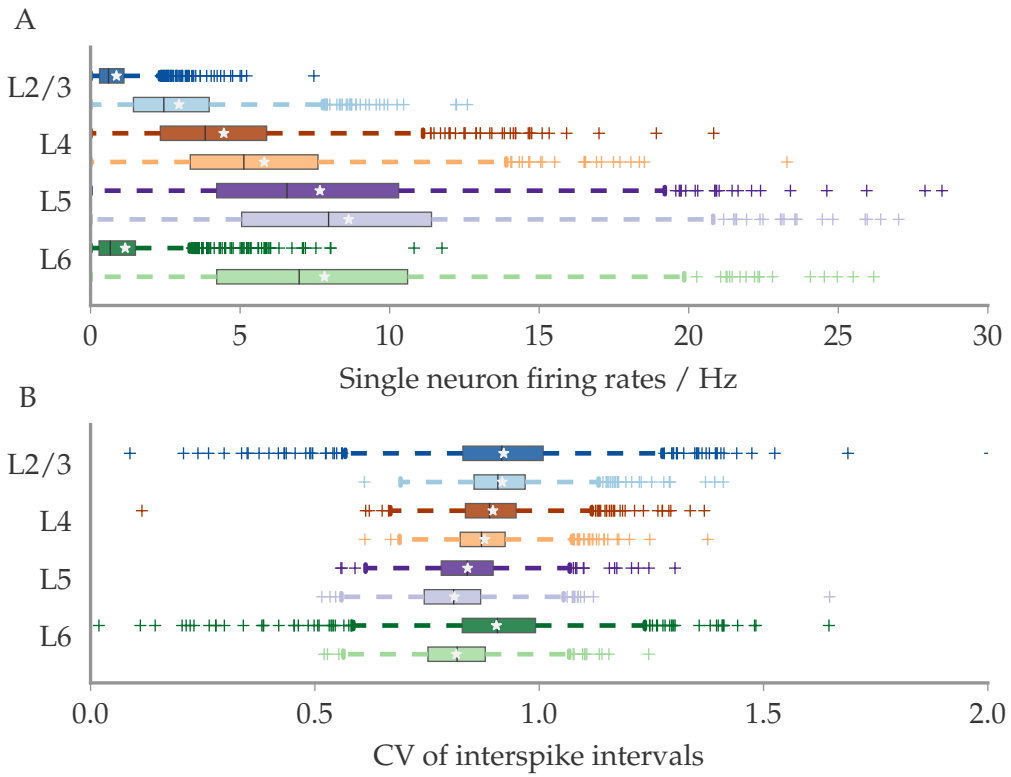

Figure 7: Single neuron activity measures: (**A**) firing rates and (**B**) CV of ISI The data is take from one simulation of the PyNEST implementation, corresponding to a single initialization in Figure 6. Statistical fluctuations are indicated by the interquartile ranges (IQR) (boxes extend to the first and third quartile). The median is indicated by a black line, the population mean by a star and whiskers extend to 1.5 IQR (outliers indicated by crosses).

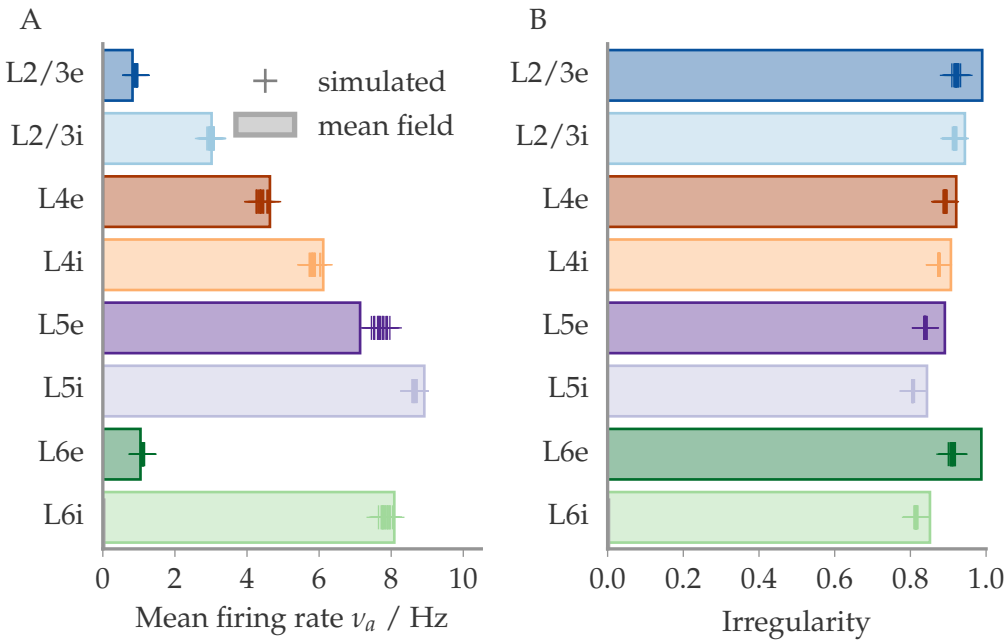

Figure 8: Comparison between mean field theory and spiking network model. Bars indicate (**A**) the single neuron firing rates and (**B**) the irregularity (mean CV of ISI) predicted by the mean field theory, crosses the respective measurements from 20 simulation (as previously shown in Figure 6). The connection for the simulations rule was set to "fixed total number".

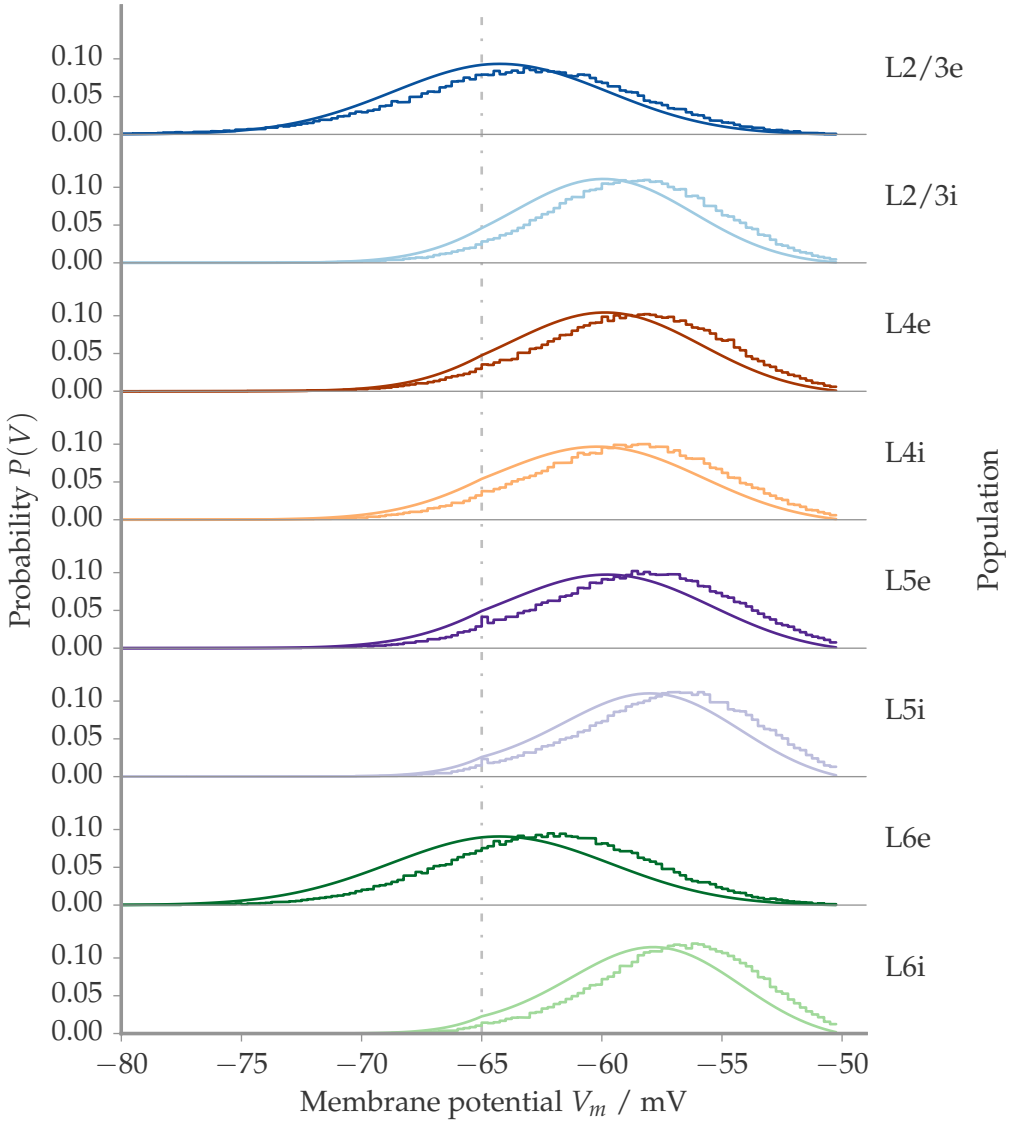

Figure 9: Distribution of membrane potentials for each population. Shown are both the results of simulation (histogram) and the predictions of the mean field theory (continuous line). The simulation results are histograms (bins width $\Delta V_m = 0.25$ mV) of membrane potential recordings of 100 neurons, recorded every 0.001 s for a simulation time of 1.0 s and adjusted for neurons in refractory period (see text). The binning in voltage is the same as applied in Fig. Figure 4. The voltage for neurons in refractory period $V_r = -65$ mV is indicated by the dashed and dotted line. The threshold is at $\theta = -50$ mV.

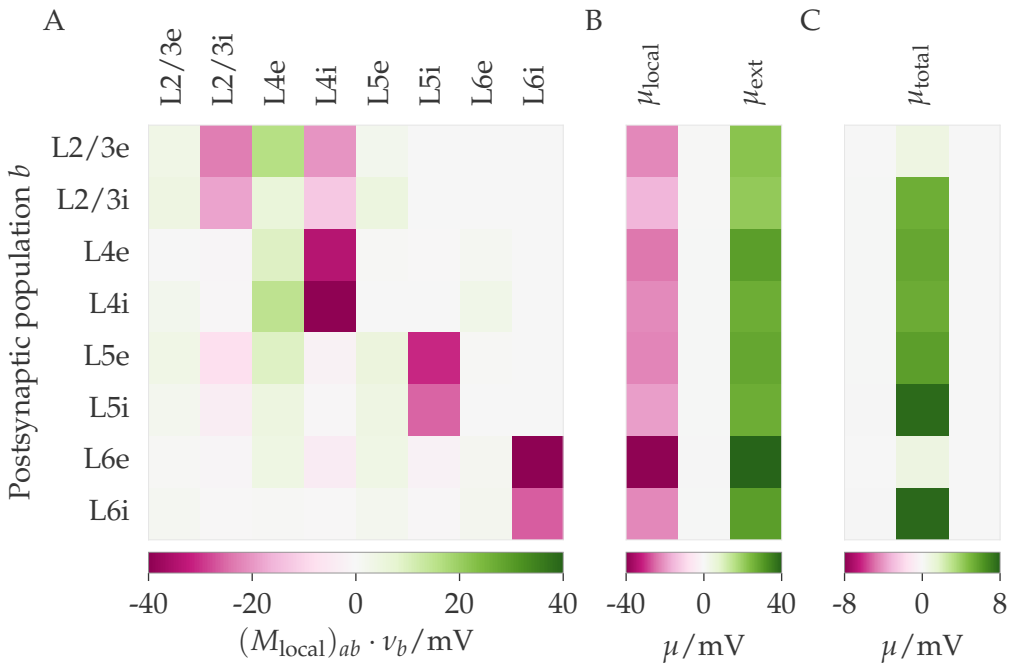

Figure 10: Mean input μ to neurons and separated constituents (see equation (55)). (**A**) The local input of each presynaptic population a (columns) to a neurons op population b (rows, postsynaptic). The first column in (**B**) corresponds to the total recurrent input μ_{local} and equals the sum of each row in (A). The second column is the external input μ_{ext}. (**C**) Total input $\mu = \mu_{\text{local}} + \mu_{\text{ext}}$. Note the different scales between (**B**) and (**C**).

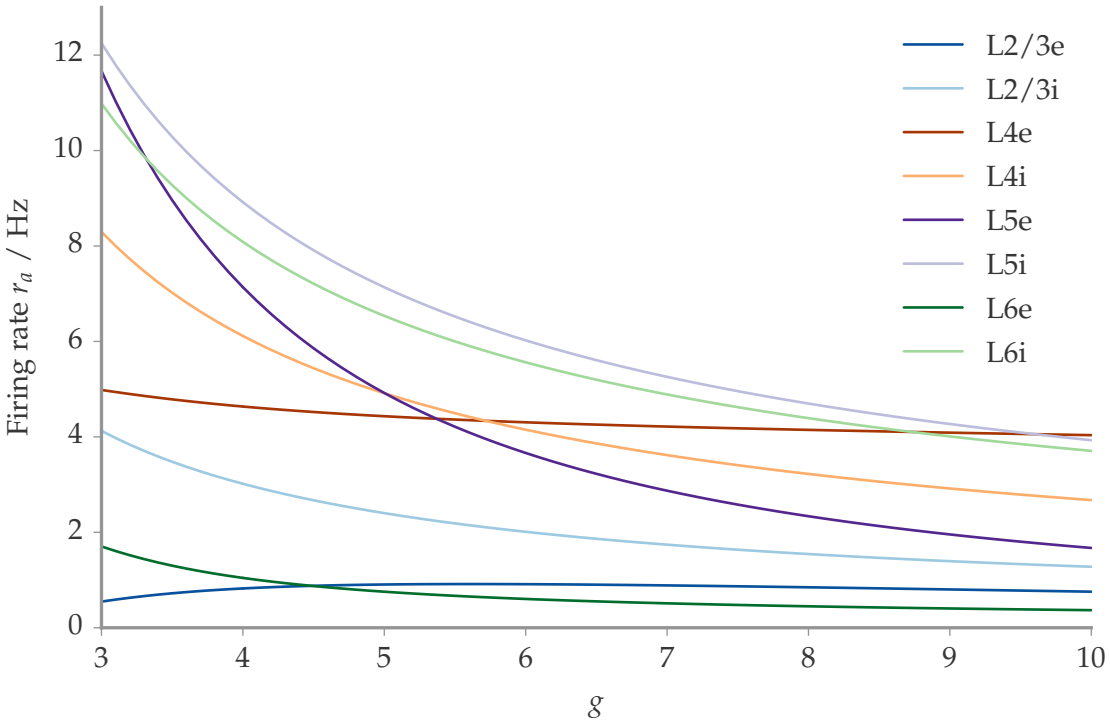

Figure 11: Firing rates for different inhibitory synaptic strength g predicted by the mean field theory. The working point of the spiking network simulation is at $g = 4$, other theoretical models use higher estimates up to $g = 8$.

4

DISCUSSION

THE REIMPLEMENTATION of Potjans and Diesmann's spiking network simulation confirmed the expectation: The original model's results were reproduced well within the statistical fluctuations. The fluctuations of the calculated population means between different instantiations of the model are relatively small, a characteristic that can be interpreted as an indication that a mean field approach is suited well for describing the corresponding network: The parameters describing the main features of the network activity depend strongly on average input and connection numbers, and much less on the actual wiring. However, this assertion has to be restricted to random networks, as more detailed structure, for example induce by learning, can lead to stronger effects of correlation (see for example Staude et al. [31]). For a single simulation, the fluctuations along neurons within one population were shown to be large both for the firing rate and the CV of ISI. This can be tracked back to the large deviations of input between different neurons: Due to randomly choosing the synapses and adding further variability by distributing the synapse number (as shown for model validation, see Methods, Section 2.1), some neurons will receive more excitatory or inhibitory input than others and fire accordingly. Since the results reproduce those of the original study, the according characterization of the network holds as well: The network activity is labeled as asynchronous irregular, with a mean CV of ISI above 0.8 and the applied synchrony measure ranging from values below 2 (populations L5i, L6e and L6i), up to ~ 8 for L5e. Still, the larger values of synchrony indicate that the amount of correlation might not be negligible for the spike rate. This has to be taken into account when interpreting the results of the mean field model.

INTRODUCING THE MEAN FIELD THEORY for the simulated spiking network turned out to be remarkably successful. The formal extension from the original model of two populations has been a rather small step, while the incorporation of further details as well as the numerical implementation revealed a number of obstacles. The resulting algorithm, nonetheless, is

a convenient and computationally inexpensive tool for predictions. It has been shown to predict central quantities of the network activity to a high degree of accuracy.

The predicted single neuron firing rates differ by less than 0.3 Hz for all populations but L5e (0.6 Hz lower than measured). Except for the latter and L2/3e, the relative error is below 7 %. In most cases, the rates are slightly lower than the measured ones.. One reason for this underestimation could be the negligence of correlation: Larger correlations among excitatory input can lead to higher fluctuations and thus higher spiking rates [31]. This assertion has to be taken with care, though, as correlation in inhibitory populations may cancel the effect as shown e. g. by Renart et al. [25].

The prognosis for the irregularity of spike trains, measured by the coefficient of variation of interspike intervals (CV of ISI) turns out to be evenly accurate: For all populations, the deviation between theory and simulation is of the order of 0.05, the largest being observed for the populations L2/3e and L6e with 0.07 and 0.08. The latter ones are the populations firing at the lowest rate. The general overestimation of irregularity can be interpreted in two ways. One explanation for the remaining differences can be an estimation bias of the CV of ISI using spike trains of finite lengths arising as a significant ratio of the neurons in the population is either not included at all (if the number of spikes is < 2) or the part of the distribution covering higher CV of ISI is not represented well (see Nawrot [22] for details). This is especially critical for the populations with low rates (L2/3e, L6e), which indeed do show the largest deviations. What cannot be accounted for by this bias would indicate a lower irregularity than that of the respective stationary Gaussian process. This points towards temporal correlations introduced for example by the synapse model beyond the effects accounted for (see e. g. Brunel and Hakim [9] for the case of α synapses in a simpler context).

The third and last measure predicted by the mean field model, the distribution of membrane potentials, also agrees well with the obtained simulation data. Both the shape and position of the distribution are reproduced. The kink at the resting potential V_r due to neurons exiting the refractory period is reproduced but less pronounced than the measured one. This indicates that the diffusion away from this point is slower than assumed. The maxima of the predicted distributions are slightly shifted towards the resting potential. Again, the interpretation

of the distribution has to be done with care: A lower maximum does not correspond to lower firing rates. The populations of layer 5 illustrate this: While for both, the shift in membrane potential is about equal, the excitatory firing rate is underestimated whereas the inhibitory one is overestimated. In the mean field model, this is reflected by relating the firing rate only to the probability current at the threshold θ, not to the shape of the curve at other points (cf. Equation 23 and following). Further, higher firing rates due to correlations are not detectable in the membrane potential distribution: Even if the membrane potential spends most time close to the resting potential, a large number of excitatory spikes arriving in a short time would lead to a quick rise and firing without affecting the distribution significantly.

The example for applying the mean field range for a range of different inhibitory synapse strengths g showed that it is a convenient tool for predicting network behavior. This is especially of use since simulating a network is tied to high computational costs and waiting time. When applying the model in this manner, the underlying assumptions have to be kept in mind in order to not leave the range of validity.

IN SUMMARY, the hypothesis for the analytical ansatz is confirmed: The considered activity measures of the simulated spiking network model of the neocortex can be predicted by a mean field theory assuming uncorrelated Gaussian input. Possible explanations for the remaining deviations are (i) correlations between neurons, yielding an input to single neurons different from the assumed white Gaussian noise; (ii) temporal correlations induced by the synapse type different from the delta synapses of the mean field model; and finally (iii) fluctuations in the input of single neurons.

The value of the analytical framework developed is twofold: On the one hand, it provides a useful tool for predicting the activity of a spiking network model over a large range of parameters On the other hand, it represents an essential means for identifying relevant measures and understanding the emergent dynamics of the complex systems under consideration. This is a hard and one of the most important tasks in this field. The long lasting debate over whether neural coding is rate based or exploits precise timing and correlations may at some point be solved by excluding one or the other option using a sensible framework of biological data, spiking network simulation and

analytical arguments. On a less ambitious scale, the presented models can at least indicate by how much correlations effect the observed rates.

The presented combination of the spiking network model and the mean field approach serves as a framework to tackle further questions. The implementation in PyNEST works as a convenient basis for extensions such as the inclusion of newly available experimental data. Furthermore, different neuron populations, especially concerning different interneuron classes, may be included, making the simulation a viable means for testing hypothesis about their role. Another possible extension already introduced in the original model [24] is unspecific input from a thalamic population. When applying this input for short bursts (e. g. 10 ms), this can by used in order to examine the way increased spike rates are propagated along the different layers in time and thus assessing the path of information processing within the neocortex. The mean field approach, however, would have to be extended to a non-equilibrium regime since it lacks temporal resolution at the present state. Finally, when focusing on neural computation, one might also include specific input. An interesting context is orientation selectivity, using oriented input resulting in neuronal tuning curves. To this end, the mean field approach can be extended to single neurons as implemented for example by Sadeh and Rotter [29] for the case of one excitatory and one inhibitory population.

BIBLIOGRAPHY

[1] BA thesis repository, Schuessler, 2015. URL https://github.com/alfred-s/microcircuit/tree/master/analysis.

[2] A notebook viewer for IPython notebooks, 2015. URL http://nbviewer.ipython.org/github/alfred-s/microcircuit/tree/master/analysis/.

[3] Daniel J Amit and Nicolas Brunel. Model of global spontaneous activity and local structured activity during delay periods in the cerebral cortex. *Cerebral cortex*, 7(3):237–252, 1997.

[4] Mark F Bear, Barry W Connors, and Michael A Paradiso. *Neuroscience: Exploring the brain*, volume 2. Lippincott Williams & Wilkins, 2007.

[5] Clemens Boucsein, Martin Nawrot, Philipp Schnepel, and Ad Aertsen. Beyond the cortical column: abundance and physiology of horizontal connections imply a strong role for inputs from the surround. *Frontiers in Neuroscience*, 5: 32, 2011.

[6] Romain Brette. What is the most realistic single-compartment model of spike initiation? 2015.

[7] K Brodmann. Vergleichende Lokalisationslehre der Großhirnrinde. *Leipzig: Barth*, 1909.

[8] Nicolas Brunel. Dynamics of sparsely connected networks of excitatory and inhibitory spiking neurons. *Journal of computational neuroscience*, 8(3):183–208, 2000.

[9] Nicolas Brunel and Vincent Hakim. Fast global oscillations in networks of integrate-and-fire neurons with low firing rates. *Neural computation*, 11(7):1621–1671, 1999.

[10] Javier DeFelipe, Henry Markram, and Kathleen S Rockland. The neocortical column. *Frontiers in neuroanatomy*, 6, 2012.

[11] John Eccles. From electrical to chemical transmission in the central nervous system. *Notes and records of the Royal Society of London*, pages 219–230, 1976.

[12] Sami El Boustani, Martin Pospischil, Michelle Rudolph-Lilith, and Alain Destexhe. Activated cortical states: experiments, analyses and models. *Journal of Physiology-Paris*, 101(1):99–109, 2007.

[13] Marc-Oliver Gewaltig and Markus Diesmann. NEST (NEural Simulation Tool). *Scholarpedia*, 2(4):1430, 2007.

[14] Alan L Hodgkin and Andrew F Huxley. A quantitative description of membrane current and its application to conduction and excitation in nerve. *The Journal of physiology*, 117(4):500–544, 1952.

[15] Jonathan C Horton and Daniel L Adams. The cortical column: A structure without a function. *Philosophical Transactions of the Royal Society B: Biological Sciences*, 360(1456): 837–862, 2005.

[16] David H Hubel and Torsten N Wiesel. Receptive fields, binocular interaction and functional architecture in the cat's visual cortex. *The Journal of physiology*, 160(1):106, 1962.

[17] J. D. Hunter. Matplotlib: A 2d graphics environment. *Computing In Science & Engineering*, 9(3):90–95, 2007.

[18] Eric Jones, Travis Oliphant, Pearu Peterson, et al. SciPy: Open source scientific tools for Python, 2001–. URL `http://www.scipy.org/`.

[19] Louis Lapicque. Recherches quantitatives sur l'excitation électrique des nerfs traitée comme une polarisation. *J. Physiol. Pathol. Gen*, 9(1):620–635, 1907.

[20] Vernon B Mountcastle. Modality and topographic properties of single neurons of cat's somatic sensory cortex. *Journal of neurophysiology*, 20(4):408–434, 1957.

[21] Martin P Nawrot, Clemens Boucsein, Victor Rodriguez Molina, Alexa Riehle, Ad Aertsen, and Stefan Rotter. Measurement of variability dynamics in cortical spike trains. *Journal of neuroscience methods*, 169(2):374–390, 2008.

[22] Martin Paul Nawrot. Analysis and interpretation of interval and count variability in neural spike trains. In *Analysis of parallel spike trains*, pages 37–58. Springer, 2010.

[23] Eilen Nordlie, Marc-Oliver Gewaltig, and Hans Ekkehard Plesser. Towards reproducible descriptions of neuronal network models. *PLoS Comput. Biol*, 5(8):e1000456, 2009.

[24] Tobias C Potjans and Markus Diesmann. The cell-type specific cortical microcircuit: Relating structure and activity in a full-scale spiking network model. *Cerebral cortex*, 24(3): 785–806, 2014.

[25] Alfonso Renart, Jaime de la Rocha, Peter Bartho, Liad Hollender, Néstor Parga, Alex Reyes, and Kenneth D Harris. The asynchronous state in cortical circuits. *science*, 327 (5965):587–590, 2010.

[26] Luigi M Ricciardi. *Diffusion processes and related topics in biology*, volume 14. Springer Science & Business Media, 2013.

[27] Guido Rossum. Python reference manual. Technical report, Amsterdam, The Netherlands, The Netherlands, 1995.

[28] Stefan Rotter and Markus Diesmann. Exact digital simulation of time-invariant linear systems with applications to neuronal modeling. *Biological cybernetics*, 81(5-6):381–402, 1999.

[29] Sadra Sadeh and Stefan Rotter. Orientation selectivity in inhibition-dominated networks of spiking neurons: Effect of single neuron properties and network dynamics. *PLoS computational biology*, 11(1):e1004045, 2015.

[30] Sadra Sadeh, Stefano Cardanobile, and Stefan Rotter. Mean-field analysis of orientation selectivity in inhibition-dominated networks of spiking neurons. *SpringerPlus*, 3 (1):148, 2014.

[31] Benjamin Staude, Sonja Grün, and Stefan Rotter. Higher-order correlations and cumulants. In *Analysis of parallel spike trains*, pages 253–280. Springer, 2010.

[32] Henry C Tuckwell. *Introduction to theoretical neurobiology: Volume 2, Nonlinear and stochastic theories*, volume 8. Cambridge University Press, 2005.

[33] Carl van Vreeswijk. Stochastic models of spike trains. In *Analysis of Parallel Spike Trains*, pages 3–20. Springer, 2010.

ACKNOWLEDGMENTS

I am indebted to Stefan Rotter and Benjamin Merkt for introducing me into the fascinating field of computational neuroscience, always being open for questions and triggering most fruitful discussions. I further want to thank Jens Timmer for his supervision. Finally, I am grateful for the support of both my family and friends, without which this work would not have been possible.

ABSTRACT

In the search for understanding the basic functions of the neocortex, linking the anatomical structure to population dynamics has been a mayor focus of research. Experimental data regarding local connectivity and cell-type specific activity is increasing at a fast pace but remains mainly inconclusive. Simultaneously, spiking network models based on leaky integrate-and-fire neurons are used for interpreting experimental data such as firing rates, correlations or oscillations. On the other hand, a deeper understanding is reached by an analytical framework relying on a statistical description. A rate based mean field theory has been developed for neural networks of two populations by Brunel [8] and successfully applied to a number spiking network models. However, for networks with many populations it is not a priori clear whether this description is adequate. One important case considered in this work is the modeling of the neocortical networks. These networks are organized in layers, a feature thought to be crucial for the information processing and thus for higher cognitive functions. A spiking network model of a substructure, termed as the local cortical microcircuit, and incorporating this characteristic was established by Potjans and Diesmann [24] in 2014. To this end, they integrated a large number of the experimental studies available and reproduced some of the main features of spiking activity observed *in vivo*. In this thesis, the spiking network model of the microcircuit is successfully reimplemented, compared with the original one and further analyzed. Aiming for a more thorough understanding, the existing mean field theory is extended to a layered network of eight populations. The predictions, namely single neuron firing rates, membrane potential distributions as well as the irregularity of spike trains, are are shown to agree with the simulated counterparts. Finally, the developed mean field theory is shown to be a convenient tool exploring the network's activity for changing parameters.

ZUSAMMENFASSUNG

Bei der Erforschung des Neokortex ist die Verbindung zwischen Struktur und Funktion der zentrale Ansatz der Computational Neuroscience. Trotz wachsender Zahl an experimentellen Ergebnissen zu Konnektivitäten und zellspezifischer Aktivität gibt es noch kein zusammenhängendes Bild darüber, wie die wichtigsten Funktionen zustande kommen. Gepulste neuronale Netze (SNN – spiking neural networks) mit leaky integrate-and-fire Neuronen liefern einen wichtigen Ansatz, um die experimentellen Daten, wie etwa Feuerraten, Korrelationen oder Oszillationen, zu verstehen. Gleichzeitig wird versucht, ein umfassenderes Verständnis mit Hilfe von statistischen Modellen zu erlangen. Von Brunel [8] wurde eine ratenbasierte Molekularfeldnäherung für Netwerke aus zwei Populationen entwickelt und bis dato auf einige SNNs angewandt. Es ist jedoch nicht klar, in wie weit diese Beschreibung auf komplexere Netzwerke verallgemeinerbar ist. Ein wichtiger Fall, der in dieser Arbeit betrachtet wird, sind Modelle neokortikaler Netzwerke. Diese sind in Schichten aufgebaut – ein Eigenschaft, die als maßgeblich für die Informationsverarbeitung und damit für höhere kognitive Fähigkeiten gilt, welche in diesem Teil des Gehirns zustandekommen. Ein SNN für den lokalen kortikalen Schaltkreis, eine Unterstruktur des Neocortex, wurde von Potjans and Diesmann [24] entwickelt. Dieses enthält die laminare Struktur. Für die Konnektivitätsmatrix des Modells wurde eine Vielzahl experimenteller Studien ausgewertet, und schließlich wurden einige wichtige Merkmale von *in vivo* gemessenen Daten reproduziert. In dieser Arbeit wird das Modell neu implementiert, mit dem Original verglichen und weitergehen untersucht. Um das Modell besser zu verstehen wird die Molekularfeldtheorie auf ein geschichtetes Netzwerk aus acht Populationen erweitert. Beim Vergleich von vorgesagten und gemessenen Daten wird gezeigt, dass die Theorie gut mit der Simulation übereinstimmt. Speziell werden dafür die Feuerraten, die Membranpotentiale und die Unregelmäßigkeit der Neuronenaktivität untersucht. Schließlich wird gezeigt, dass sich die Molekularfeldtheorie auch als nützliches Werkzeug zur weiteren Untersuchung bei veränderten Netzwerkparametern eignet.